J. Fluid Mech. (2003), *vol.* 495, *pp.* 283–321.
DOI: 10.1017/S002211200300630X Printed in the United Kingdom

A multiphase model with internal degrees of freedom: application to shock–bubble interaction

By RICHARD SAUREL[1]†, SERGEY GAVRILYUK[2] AND FRANÇOIS RENAUD[3]

[1]Institut Universitaire de France and Polytech Marseille, UMR CNRS 6595 IUSTI, 5 rue E. Fermi, 13453 Marseille Cedex 13, France

[2]LMMT, Université Aix Marseille III, case 322, Av. Escadrille Normandie-Niemen, 13397 Marseille Cedex 20, France

[3]CEA/DIF BP 12, 91680 Bruyères le Châtel, France

Richard.Saurel@polytech.univ-mrs.fr; sergey.gavrilyuk@univ.u-3mrs.fr; francois.renaud@cea.fr

(Received 22 July 2002 and in revised form 1 July 2003)

The aim of this paper is the derivation of a multiphase model of compressible fluids. Each fluid has a different average translational velocity, density, pressure, internal energy as well as the energies related to rotation and vibration. The main difficulty is the description of these various translational, rotational and vibrational motions in the context of a one-dimensional model. The second difficulty is the determination of closure relations for such a system: the 'drag' force between inviscid fluids, pressure relaxation rate, vibration and rotation creation rates, etc. The rotation creation rate is particularly important for turbulent flows with shock waves. In order to derive the one-dimensional multiphase model, two different approaches are used. The first one is based on the Hamilton principle. This method gives thermodynamically consistent equations with a clear mathematical structure, coupling the various motions: translation, rotation and vibration. However the relaxation effects have to be added phenomenologically. In order to achieve the closure of the system and its numerical resolution we use the second approach, in which the pure fluid equations are discretized at the microscopic level and then averaged. In this context, the flow is considered to be the annular flow of two turbulent fluids. We also derive the continuous limit of this model which provides explicit formulae for the closure laws. The structure of this system of partial differential equations is the same as the one obtained by the Hamilton principle. The final issue is to determine the rate of energy (or entropy) rotation. We assume that all the entropy creation related to the various relaxation effects after the passage of the shock wave is converted to rotational motion. The one-dimensional model is validated by comparing its predictions with averaged two-dimensional direct numerical results. The problem on which this model is tested is the interaction of a shock wave propagating in a heavy gas with a light gas bubble. The results obtained by the one-dimensional multiphase model are in a very good agreement with the two-dimensional averaged results.

1. Introduction

In most applications with multiphase mixtures it is not possible to solve the interface problem at the scale of each individual phase. This is why a reduced averaged

† Also Projet SMASH, INRIA Sophia Antipolis

multiphase model (turbulent or not) may be useful. This reduced model must be as accurate as possible: it must involve most of the multidimensional microscale physics.

The typical example we consider in this paper is the two-dimensional shock wave interaction with a bubble with density smaller than that of ambient fluid. Both fluids have different equations of state. During this process, the Richtmyer–Meshkov instability causes bubble collapse, followed by rotation of the fluids and their translation. A reduced compressible multiphase description of this phenomenon is necessary. Such models have been developed mainly for the case when the internal inertia of the dispersed phase (bubble pulsation) and the internal fluid rotation ('turbulent effects' in a generic sense) are negligible (Stewart & Wendroff 1984; Baer & Nunziato 1986; Kapila *et al.* 1997; Saurel & Abgrall 1999*a*; Kapila *et al.* 2001; Saurel & LeMetayer 2001). Gavrilyuk & Saurel (2002) have obtained a two-fluid model for mixtures with inertia effects (for example, liquids containing small gas bubbles) by using a variational approach. All the above-mentioned models are hyperbolic. We do not discuss here non-hyperbolic models which are also used sometimes for the study of wave propagation in compressible flows. The works of Youngs (1984, 1989*a*, *b*), Gardner *et al.* (1988), Glimm *et al.* (1990), Glimm, Saltz & Sharp (1999), and Chen *et al.* (1996) deal with a multiphase approach to turbulent mixtures.

In this paper we develop two approaches to account for the internal rotation of fluids (fluid turbulence). This internal rotation is responsible for the strong localized pressure decrease occurring after the bubble compression by the shock wave. This rotation motion is associated with important storage of the mechanical energy of the system.

The first approach is based on the variational formulation of a multiphase model with internal inertia and internal rotation. We obtain a hyperbolic model for the dissipation-free case and add drag terms compatible with the second principle of thermodynamics. This approach provides a general mathematical structure of governing equations analogous to a coupled system of two compressible fluids moving in a duct of variable cross-section. The coupling equation is the equation for the volume concentration, playing the role of 'duct cross-section'. This system is not in conservative form. The right-hand sides ('nozzling' terms) represent the product of 'interface parameters' (interface pressure and velocity) with the gradient of the volume concentration, plus some other terms.

Closure of this reduced model is a difficult task. Indeed, the second principle of thermodynamics cannot determine the expression for relaxation coefficients; it determines only their sign. Moreover, the 'interface' parameters have to be prescribed *a priori*. Even if the results given by this model are in good agreement with experimental and numerical results for some test problems for a particular choice of relaxation and interface parameters (Gavrilyuk & Saurel 2002), the problem of closure remains.

This is why we present a second approach, based on the discrete equation method (DEM) proposed recently by Abgrall & Saurel (2003). The method is also a numerical one; its basic ingredients are as follows. Instead of solving a system of partial differential equations obtained after averaging of the pure fluid equations in each medium, the DEM presents, first, the pure fluid equations in discrete form in each cell, and second, averages the discrete formula (the meaning of average will be described later). The interface variables are defined through the solution of one-dimensional Riemann problems. This method presents several advantages. First, an accurate numerical approximation of the multiphase model, including non-conservative terms is obtained. Second, the 'interface parameters' present on the right-hand side of the equations are determined. Third, the relaxation parameters (pressure drag force and

pressure relaxation rate) are determined also. By examining the continuous limit of the discrete model, explicit formulae for these various closure laws are obtained. Finally, the resulting model is free of parameters.

When dealing with rotation effects, it is necessary to determine the production rate of rotation due to the shock wave interaction. This is done by examining the entropy production of the above model. More specifically, we assume that the rotation motion appearing after the passage of the shock wave is such that the thermodynamic entropy of each fluid does not increase in its relaxation zone; this hypothesis is plausible on the small time interaction scale. This assumption again provides a parameter-free model giving excellent agreement with the averaged two-dimensional results from a direct numerical simulation (DNS).

The paper is organized as follows. In § 2 we describe the shock–bubble test problem and the numerical method used for the two-dimensional numerical simulation. In § 3 we develop an initial form of the governing equations describing the multiphase mixture with translation, rotation and vibration obtained by the variational principle. This is a system of 10 partial differential equations (for the one-dimensional case). For the present application, vibration effects being negligible (density ratio is relatively weak), an asymptotic reduction to a nine equations model is established.

The discrete equation method (DEM) is given in § 4 for a particular two-dimensional topology, associated with the annular gas–liquid flow. This representation is a correct approximation of the shock–bubble interaction problem. In the paper by Abgrall & Saurel (2003) this method was developed to couple Euler equations valid in each phase. Here we couple the dissipation-free turbulent Euler equations (a one-equation turbulent model, or simply 'k-model'). To use the DEM, we need to solve the Riemann problem for the k-model. An approximate Riemann solver is developed in § 5.

We examine in § 6 the continuous limit of equations obtained by the DEM. The limit model possesses the same structure as the one developed in § 3 by using the Hamilton principle and asymptotic reduction. For the annular two-phase flow, the analysis determines explicit formulae for the relaxation coefficients as well as the interface variables. We obtain in § 7 the rotation (turbulent) entropy production term. Finally, in § 8 the DEM is validated numerically on several test problems including shock–bubble interaction. Mathematical details are given in Appendices.

2. Shock–bubble interaction problem and numerical experiments

The problem that will serve as illustration throughout this work and that will provide reference results for the reduced multiphase model is shock–bubble interaction. Indeed, the aim of the present study is the derivation of a one-dimensional turbulent multiphase model. To evaluate its accuracy and study basic phenomena, reference results are necessary. We propose to determine these reference results by direct numerical simulation of the two-dimensional Euler equations applied to a shock wave propagating in a heavy gas and interacting with a light gas bubble. The two fluids have different equations of state and thermodynamic variables. This is why a multiphase description will be adopted. A schematic representation of the example under study is shown in figure 1.

We study the two-dimensional shock wave interaction with a light gas bubble (in fact a square cylinder) inside a heavy gas. The physical parameters of the configuration considered are the following. The centre of mass of a square gas cylinder is located a distance 2 m along the x-axis. This cylinder is placed inside a shock tube filled with a higher density gas. The light gas is at rest and has an initial density of $1\,\mathrm{kg\,m^{-3}}$

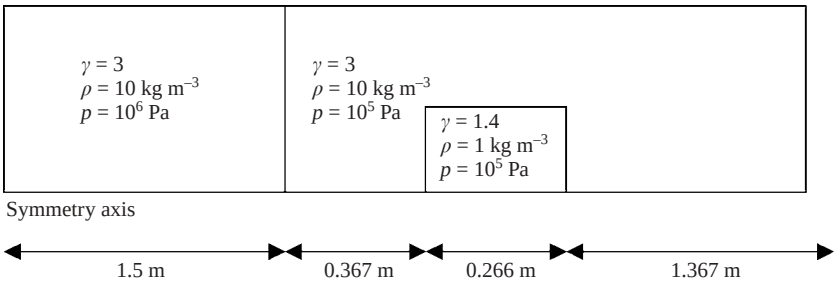

FIGURE 1. Schematic representation of the test problem under study. Shock interaction with a density discontinuity (a 'square' gas bubble). The shock propagates into a heavy fluid and interacts with a bubble of light fluid.

and a pressure of 10^5 Pa. The gas polytropic exponent is 1.4. The still heavy fluid fills the rest of the domain; its polytropic exponent is equal to 3 and initial density is $10\,\mathrm{kg\,m^{-3}}$. The high-pressure chamber (10^6 Pa) begins at $x=0$ and ends at $x=1.5$ m. The low-pressure (10^5 Pa) chamber begins at $x=1.5$ m and ends at $x=3.5$ m. This is summarized in figure 1. These parameters are chosen arbitrarily. They correspond to an incident shock Mach number equal to 1.90. Pressure, density and polytropic coefficient ratios are chosen relatively high in order that the test problem presents a strong shock wave and contact discontinuity and different thermodynamic behaviour via the equation of state, such that a single phase description is inappropriate. Such difficult conditions are also representative of specific conditions occurring in plasma physics as studied in Youngs (1984, 1989*a*, *b*), Glimm *et al.* (1990, 1999), Chen *et al.* (1996) and Gardner *et al.* (1988).

The fact that the two fluids have different equations of state is a difficulty for the two-dimensional computations due to the presence of a two-dimensional contact interface separating the fluids. In order to deal with very large deformations, we wish to solve the Euler equations by using an Eulerian method. This poses the well-known problem of artificial diffusion of contact discontinuities. At the contact interface, the density and internal energy are smeared over several mesh points. Since the interface separates media with different equations of state, the computation of pressure, sound speed and all thermodynamic variables is critical. Negative pressure can be numerically obtained, yielding failure of the computation. Fulfilment of the interface conditions is mandatory. This question has been addressed by many authors: Karni (1994, 1996); Abgrall (1996); Shyue (1998); Fedkiw *et al.* (1999); Saurel & Abgrall (1999*b*); Nguyen, Gibou & Fedkiw (2002). We have used here an extension of the approaches used by Abgrall (1996), Shyue (1998) and Saurel & Abgrall (1999*b*) as presented in Massoni *et al.* (2002). First the Euler equations are replaced by a reduced single-velocity multiphase flow model for two phases $a=1,2$:

$$\frac{\partial \alpha_a}{\partial t} + \boldsymbol{u}\cdot\nabla\alpha_a = 0, \tag{1a}$$

$$\frac{\partial \alpha_a\rho_a}{\partial t} + \nabla\cdot(\alpha_a\rho_a\boldsymbol{u}) = 0, \tag{1b}$$

$$\frac{\partial \rho\boldsymbol{u}}{\partial t} + \nabla\cdot(\rho\boldsymbol{u}\otimes\boldsymbol{u} + p\boldsymbol{I}) = 0, \tag{1c}$$

$$\frac{\partial \rho E}{\partial t} + \nabla\cdot(\boldsymbol{u}(\rho E + p)) = 0. \tag{1d}$$

This model presents a very good compromise between simplicity for the computation of interface problems and accuracy. This model and the numerical method are also conservative regarding total mass, momentum and energy. However, in extreme situations involving strong slip at interfaces, it may induce some errors on the pressure computation. When dealing with applications with strong slip effects knowledge of the velocities on both sides of the interface is necessary. These velocities are necessary to determine correctly the kinetic energy in order to computate the internal energy and pressure. The methods of Fedkiw *et al.* (1999) and Nguyen *et al.* (2002) and the multiphase approach of Saurel & Abgrall (1999*a*) and Saurel & LeMetayer (2001) can be used to compute two velocities at the interface cells. The methods of Nguyen *et al.* (2002), Saurel & Abgrall (1999*a*) and Abgrall & Saurel (2003) guarantee conservation and slip line computation. However, they are more complicated and more expensive in computational resources compared to the resolution of system (1). In the present application, sliding line effects are negligible. Thus, model (1) is preferred. Its numerical resolution is summarized below.

In this model α_a and ρ_a are the characteristic function and the density of material a. The mixture density, velocity, pressure and total energy are denoted by $\rho = \sum \alpha_a \rho_a$, u, p, E, respectively. Each pure material possesses its own equation of state (EOS) of the form $e_a = e_a(\rho_a, p_a)$. The internal energy of the mixture is obtained from the total energy of the system: $e = E - \frac{1}{2}|\boldsymbol{u}|^2$.

In order to fulfil numerically the interface conditions (equal pressures and normal velocities) the numerical viscosity of the non-conservative scheme for the numerical resolution of (1*a*) must be compatible with the one used to solve the conservative part of system (1). This compatibility condition between the two schemes is explained in Saurel & Abgrall (1999*b*). Let us recall the main formulae in the one-dimensional case for simplicity. The conservative part of the system is

$$\frac{\partial \boldsymbol{U}}{\partial t} + \frac{\partial \boldsymbol{F}(\boldsymbol{U})}{\partial x} = \boldsymbol{0}$$

where $\boldsymbol{U} = (\alpha_a \rho_a, \rho \boldsymbol{u}, \rho E)^T$ is the conservative variables vector and $\boldsymbol{F}(\boldsymbol{U})$ the associated flux. To solve this system, the Godunov scheme (or its higher-order variants) is used:

$$\boldsymbol{U}_i^{n+1} = \boldsymbol{U}_i^n - \lambda\left(\boldsymbol{F}^*_{i+1/2} - \boldsymbol{F}^*_{i-1/2}\right)$$

where $\boldsymbol{U}_i$ is the mean value of $\boldsymbol{U}$ in cell i, $\boldsymbol{F}^*_{i\pm1/2}$ is the flux solution of the exact or approximate Riemann problem. The ratio between the time step and cell size is denoted by $\lambda = \Delta t/\Delta x$. The superscripts n and $n+1$ denote two consecutive time steps. The subscripts $i + 1/2$ and $i - 1/2$ are related to right- and left-hand computational cell boundaries.

When the Godunov scheme is used for the integration of the conservative part of system (1), it is of paramount importance that the characteristic function equation also be solved by the Godunov scheme for the advection equations:

$$\alpha_i^{n+1} = \alpha_i^n - \lambda\left((u\alpha)^*_{i+1/2} - (u\alpha)^*_{i-1/2} - \alpha_i^n\left(u^*_{i+1/2} - u^*_{i-1/2}\right)\right).$$

In this formula, α^* is computed with a Riemann solver for the Euler equations and upwinded according to the contact discontinuity velocity u^*. Note that the calculated value of the characteristic function is the cell average and thus α is the volume fraction. To proceed to the next time step we have to determine the mixture thermodynamic variables. The mixture pressure is obtained from the definition of the total energy: $\rho e = \sum \alpha_a \rho_a e_a(\rho_a, p_a)$. Under the assumption of pressure equilibrium $p_1 = p_2 = p$ this

FIGURE 2. Density contours from the direct numerical simulation of the shock interaction with the light gas bubble. Results are shown at times (*a*) 2.91 ms, (*b*) 5.24 ms, (*c*) 7.66 ms and (*d*) 9.66 ms.

equation contains a single unknown p. For instance, when each material is governed by the stiffened gas EOS

$$e_a(\rho_a, p_a) = \frac{p_a + \gamma_a p_{\infty,a}}{\rho_a(\gamma_a - 1)},$$

the mixture pressure is

$$p = \frac{\rho e - \sum \dfrac{\alpha_a \gamma_a p_{\infty,a}}{\gamma_a - 1}}{\sum \dfrac{\alpha_a}{\gamma_a - 1}}$$

where γ_a and $p_{\infty,a}$ are characteristic parameters of each material.

The computation of the situation shown in figure 1 is performed with a two-dimensional extension of the previous method with directional splitting, second-order time and space accuracy with the MUSCL Hancock strategy. The various ingredients are explained in Saurel & Abgrall (1999*b*) in the context of a simplified version of (1). For an introduction to Godunov-type methods and Riemann solvers the reader is referred to the excellent book of Toro (1997).

The two-dimensional evolution of the density field is shown in figure 2 at times 2.91 ms, 5.24 ms, 7.66 ms and 9.66 ms. A mesh composed of 1050 cells in the x-direction and 90 cells in the y-direction is used. Figure 2(*a*) shows the initial stage of the shock interaction with the bubble. The bubble deformation begins with a Richtmyer–Meshkov instability that develops along the x-axis. On figure 2(*b*) the transmitted shock wave has been completely reconstructed. The bubble is now highly deformed. The first jet on the symmetry axis has caused a first bubble rupture. The secondary bubble is compressed again by another Richtmyer–Meshkov instability

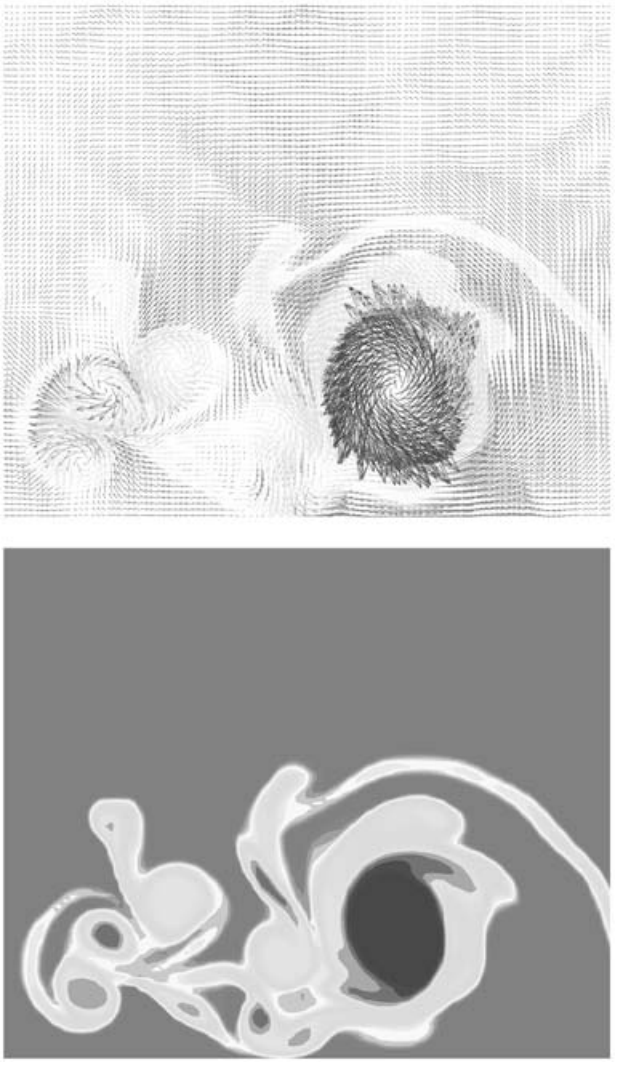

FIGURE 3. Magnified view of the velocity vectors (top) and volume fraction contours (bottom) from the direct numerical simulation of the shock interaction with the light gas bubble after the shock reflection from the tube end. The bubble is highly deformed. The fluids have an intense rotating motion. Results are shown at time 9.66 ms.

which causes another rupture. From figure 2(*b*) to the end the bubbles undergo intense rotation. On figure 2(*d*), the bubble is compressed again, as is the entire flow at the end of the shock tube, due to the shock wave reflection at the wall boundary. From this figure, we see that at least one rotation motion has to be considered in the light fluid and must be taken into account in the one-dimensional multiphase model. From a magnified view of the velocity vectors inside and outside the bubble (figure 3), it appears that the heavy fluid also has some kind of rotating (turbulent) motion. This magnified view is at the same instant as figure 2(*d*) (9.66 ms). Figure 3 shows the velocity field and the volume fraction contours.

These two-dimensional results are now averaged over each cross-section of the shock tube. Then we define the mixture density $\langle\rho\rangle(x,t)$, the mixture pressure $\langle p\rangle(x,t)$, the

mixture velocity $\langle \boldsymbol{u} \rangle(x,t)$, the phase volume fraction $\langle \alpha_a \rangle(x,t)$, the phase velocity $\langle \boldsymbol{u}_a \rangle(x,t)$, the phase pressure $\langle p_a \rangle(x,t)$ and the phase internal energy $\langle e_a \rangle(x,t)$ by the formulae:

$$\langle \rho \rangle(x,t) = \frac{\int_0^H \sum \alpha_a \rho_a \, \mathrm{d}y}{H}, \quad \langle p \rangle(x,t) = \frac{\int_0^H p \, \mathrm{d}y}{H}, \quad \langle \boldsymbol{u} \rangle(x,t) = \frac{\int_0^H \rho \boldsymbol{u} \, \mathrm{d}y}{\langle \rho \rangle H},$$

$$\langle \alpha_a \rangle(x,t) = \frac{\int_0^H \alpha_a \, \mathrm{d}y}{H}, \quad \langle \boldsymbol{u}_a \rangle(x,t) = \frac{\int_0^H \alpha_a \rho_a \boldsymbol{u}_a \, \mathrm{d}y}{\int_0^H \alpha_a \rho_a \, \mathrm{d}y},$$

$$\langle p_a \rangle(x,t) = \frac{\int_0^H \alpha_a p \, \mathrm{d}y}{\int_0^H \alpha_a \, \mathrm{d}y}, \quad \langle e_a \rangle(x,t) = \frac{\int_0^H \alpha_a \rho_a e_a \, \mathrm{d}y}{\int_0^H \alpha_a \rho_a \, \mathrm{d}y}.$$

The corresponding averaged variables are shown in figures 4, 5 and 6. All these averaged two-dimensional results will serve as a reference solution for the one-dimensional two-phase model.

On the first curve of the pressure graph (figure 4*a*) the shock wave has reached the bubble and is strongly modified by the interaction. If the bubble were absent the pressure jump would be of 5 atm, where here it is 4 atm. The main rarefaction wave travels into the high-pressure chamber and is not sensitive to what occurs in the low-pressure chamber. It is important to note the appearance of a secondary rarefaction wave facing left in the direction of the high-pressure chamber. This rarefaction wave is due to the 'bubble' volume compression. In later instants, this wave train is quasi-stationary.

After the interaction with the bubble, the shock wave reaches a pressure value close to the one it would have if the bubble were absent. On the second pressure graph (figure 4*b*) the main rarefaction wave exits the domain. At the bubble location, a low-pressure zone is visible. This new quasi-stationary local depression is convected to the right. On the third pressure graph (figure 4*c*) the leading shock wave reflects from the wall boundary. On the figure 4(*d*), the reflected shock wave has interacted with the rotating bubbles, compressing them again (see the volume fraction graphs in figure 5). The goal of the present paper is to derive a one-dimensional model that predicts the same results.

With the two-dimensional direct numerical simulation we are also able to draw the flow variables in each fluid, light or heavy. Averaged phase pressures and velocities are shown in figure 6 at time 5.24 ms (as in figure 2*b*). From these results important features of the averaged two-dimensional flow can be noticed:

(i) The light and heavy fluids have two distinct translation velocities, so that the one-dimensional model must involve at least two translation velocities. The bubble translation velocity being not necessarily equal to one of these velocities, an extra translation velocity might be necessary.

(ii) The averaged pressures are not in equilibrium inside and outside the bubbles. Some differences are visible in figure 6 .

(iii) The volume fraction strongly decreases from the initial state to the nearly equilibrium state of the final time. The one-dimensional model must consequently involve a radial or collapse velocity, responsible for volume variations.

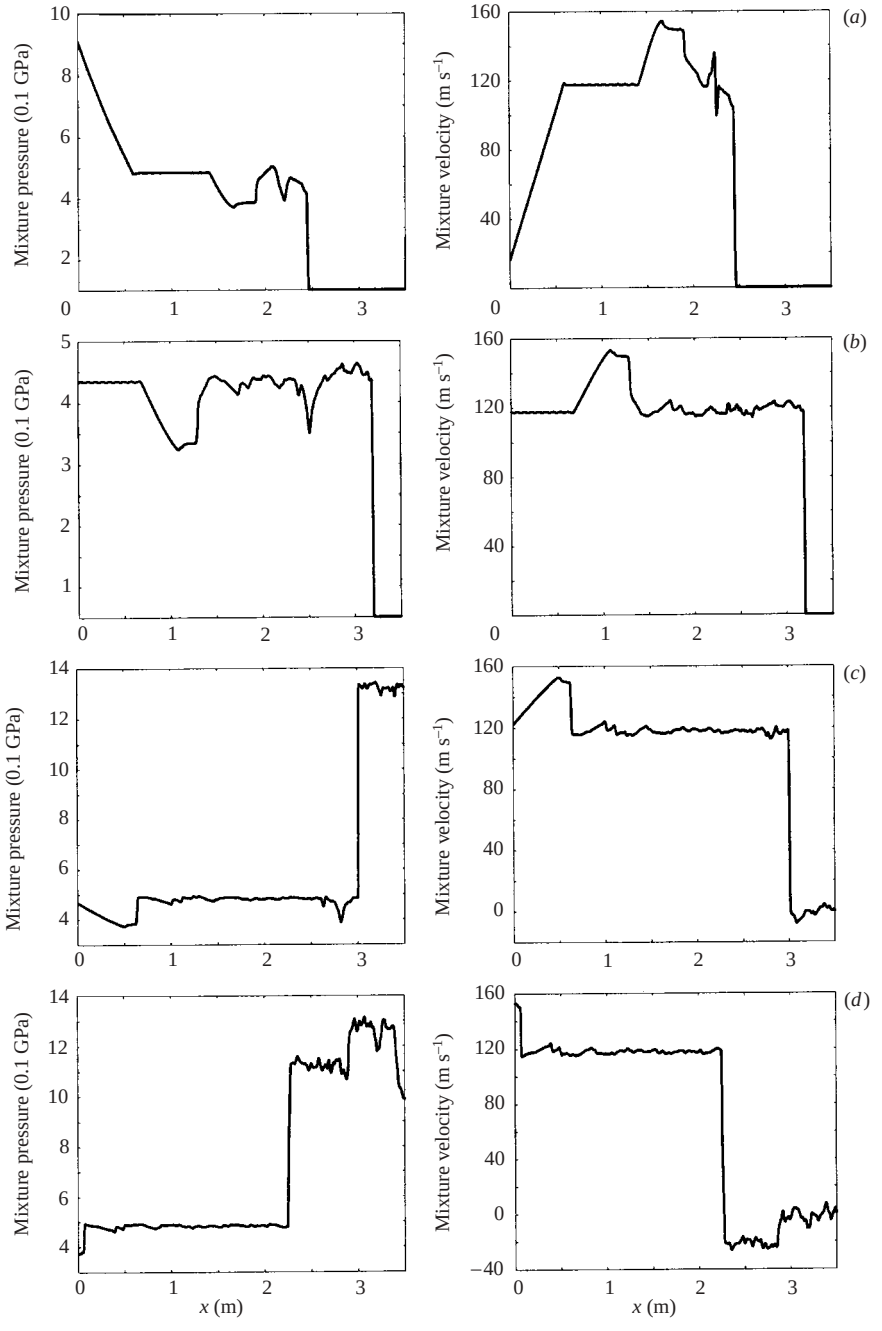

FIGURE 4. Averaged mixture pressure and velocity at times (*a*) 2.91 ms, (*b*) 5.24 ms, (*c*) 7.66 ms and (*d*) 9.66 ms.

(iv) The rotation motion in both fluids must be considered (figure 3). It is responsible for a strong pressure decrease in each fluid at the bubble location (see, for example, the pressure graph in figure 6). It is also important to note that the pressure decrease is stationary and convected with the bubble motion (figure 4).

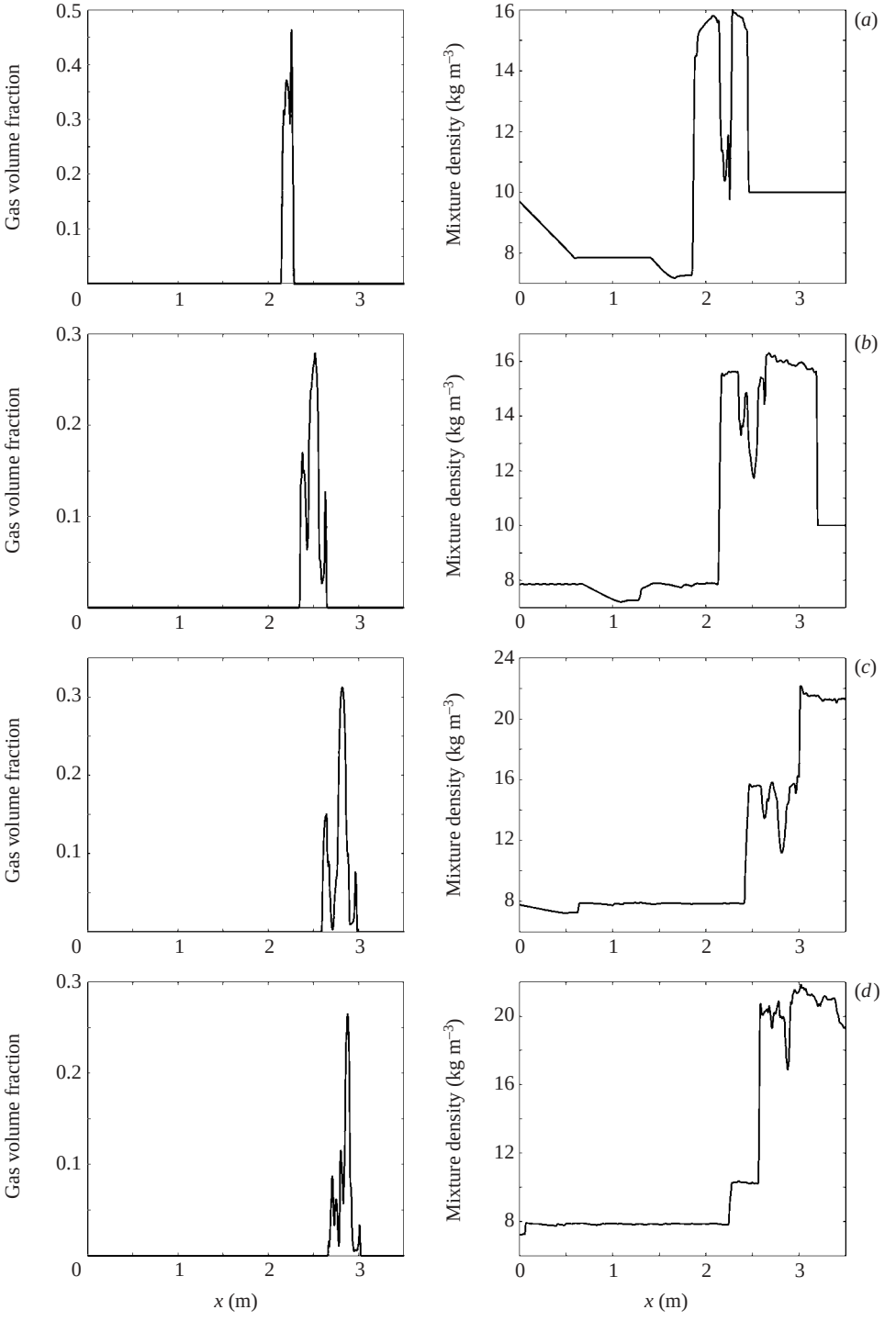

FIGURE 5. Averaged mixture density and light fluid volume fraction at times (*a*) 2.91 ms, (*b*) 5.24 ms, (*c*) 7.66 ms and (*d*) 9.66 ms.

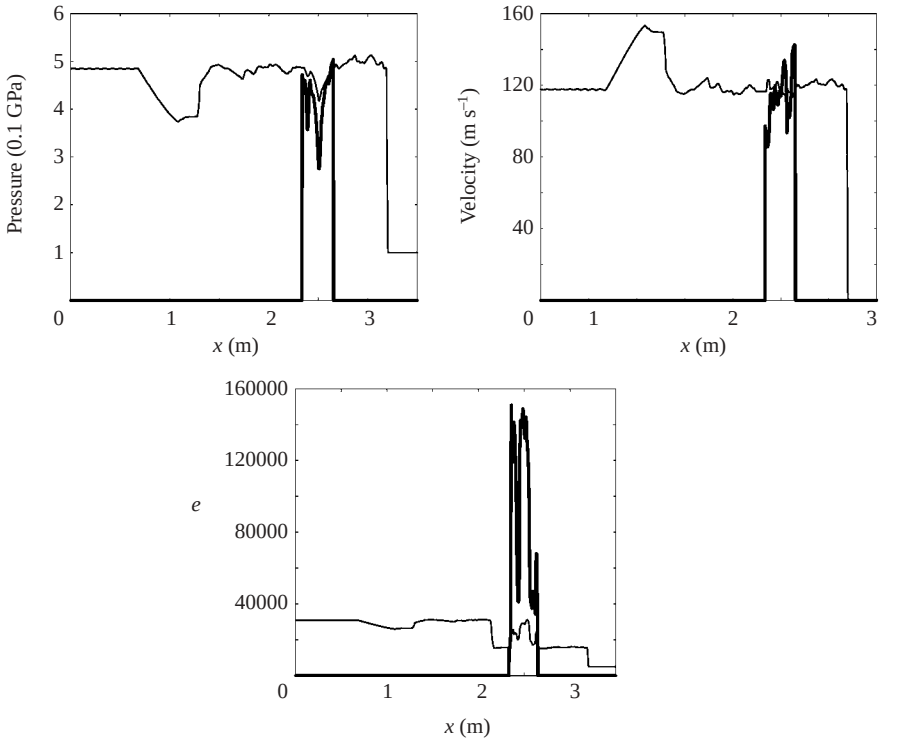

FIGURE 6. Averaged fluid pressures, velocities and internal energies at time 5.24 ms.

In the next Section we develop the arguments used for the construction of the one-dimensional model involving these features.

3. Turbulent multiphase model of compressible fluids

In this Section, the approach developed for the turbulence-free case in Gavrilyuk & Saurel (2002) is modified to account for the internal rotation inside each component. The method is based on Hamilton's principle of stationary action.

We will use the following notation. Let 2 denote the dispersed phase and 1 the continuous phase. Each ath component ($a = 1, 2$) has its own averaged characteristics: the local velocity $\boldsymbol{u}_a$; the local densities ρ_a; the partial densities $\bar{\rho}_a = \alpha_a \rho_a$, where α_a is the volume fraction of the ath component, $\alpha_1 + \alpha_2 = 1$; the local entropy per unit mass η_a; the local internal energy per unit mass $e_a(\rho_a, \eta_a)$ and the local temperatures θ_a. Moreover, we will introduce the quantities $\varkappa_a$ which represent 'turbulent entropy' for each component (this notion will be explained later). The partial densities obey the mass conservation law

$$\frac{\partial \bar{\rho}_a}{\partial t} + \nabla \cdot (\bar{\rho}_a \boldsymbol{u}_a) = 0. \tag{2}$$

For dissipation-free motions the local entropies η_a and the turbulent entropies $\varkappa_a$ are conserved along trajectories:

$$\frac{\mathrm{d}_a \eta_a}{\mathrm{d}t} = 0, \quad \frac{\mathrm{d}_a \varkappa_a}{\mathrm{d}t} = 0, \quad \frac{\mathrm{d}_a}{\mathrm{d}t} = \frac{\partial}{\partial t} + \boldsymbol{u}_a \cdot \nabla. \tag{3}$$

The energy $e_a(\rho_a, \eta_a)$ satisfies the Gibbs identity:

$$\theta_a \mathrm{d}\eta_a = \mathrm{d}e_a + p_a \mathrm{d}\left(\frac{1}{\rho_a}\right), \tag{4}$$

where p_a is the thermodynamic pressure. As consequence of (2) and (3), the partial entropies

$$\mathscr{S}_a = \bar{\rho}_a \eta_a, \quad \mathscr{T}_a = \bar{\rho}_a \varkappa_a$$

satisfy for continuous motions the conservation laws

$$\frac{\partial \mathscr{S}_a}{\partial t} + \nabla \cdot (\mathscr{S}_a \boldsymbol{u}_a) = 0, \quad \frac{\partial \mathscr{T}_a}{\partial t} + \nabla \cdot (\mathscr{T}_a \boldsymbol{u}_a) = 0. \tag{5}$$

Whereas the notion of the entropy η_a is clear, the notion of the 'turbulent entropy' should be explained. Consider the dissipation-free k-model for compressible flows (a one-equation turbulent model) written in terms of averaged parameters (Wilcox 1998; Declerc *et al.* 2001 and others):

$$\frac{\partial \rho}{\partial t} + \nabla \cdot (\rho \boldsymbol{u}) = 0, \tag{6a}$$

$$\frac{\partial \rho \boldsymbol{u}}{\partial t} + \nabla \cdot (\rho \boldsymbol{u} \otimes \boldsymbol{u} + P\boldsymbol{I}) = 0, \tag{6b}$$

$$\frac{\partial}{\partial t}\left(\rho e + \tfrac{1}{2}\rho |\boldsymbol{u}|^2 + k\right) + \nabla \cdot \left(\boldsymbol{u}\left(\rho e + \tfrac{1}{2}\rho |\boldsymbol{u}|^2 + k + P\right)\right) = 0, \tag{6c}$$

$$\frac{\partial}{\partial t}\left(\frac{k}{\rho^{\Gamma}}\right) + \boldsymbol{u} \cdot \nabla \left(\frac{k}{\rho^{\Gamma}}\right) = 0. \tag{6d}$$

Here k is the turbulent energy, $P = p + (\Gamma - 1)k$ is the sum of the thermodynamic pressure and the turbulent pressure. The value of Γ depends on the space dimension: $\Gamma = 5/3$ for the three-dimensional case, and $\Gamma = 2$ for the two-dimensional case. The last equation of (6) represents the conservation of the quantity $\varkappa = k/\rho^{\Gamma}$ which we will call 'turbulent entropy' by analogy with the classical entropy.

It is interesting to note that model (6) can be obtained from the following variational principle. Consider the Lagrangian

$$L = \frac{\rho |\boldsymbol{u}|^2}{2} - \rho e - \rho^{\Gamma} \varkappa \tag{7}$$

subjected to the constraints

$$\frac{\partial \rho}{\partial t} + \nabla \cdot (\rho \boldsymbol{u}) = 0, \quad \frac{\mathrm{d}\eta}{\mathrm{d}t} = 0, \quad \frac{\mathrm{d}\varkappa}{\mathrm{d}t} = 0. \tag{8}$$

Then the Euler–Lagrange equations for (7)–(8) are equivalent to (6). The proof is analogous to that of Serrin (1959), who used the method of Lagrange multipliers to obtain the Euler equations of compressible fluids (see also an alternative approach in Gavrilyuk & Gouin (1999) who have obtained the governing equations for more general case by using the variations in the four-dimensional case: in space and time). It is worth emphasizing that the turbulent energy k should be considered not as part of the kinetic energy, but as part of the potential energy (the minus sign in the expression for the Lagrangian).

Remark It is important to note that the jump conditions for model (6) at the contact discontinuity are $[P] = 0$ and $[\boldsymbol{u} \cdot \boldsymbol{n}] = 0$, where $\boldsymbol{n}$ is the unit normal vector to the interface. Thus, if two space domains are separated by a contact discontinuity, and if the turbulent entropy is discontinuous across the contact surface, then the total

pressure will be continuous across this contact discontinuity while the thermodynamic pressures will be different. In other words, if the turbulent entropy inside the bubble is different from the turbulent entropy outside the bubble, then the thermodynamic pressures will be different, and this difference will be preserved when the bubble moves with the flow velocity. Thus, the local depression will be convected. This feature is important for our applications.

Our goal is to construct a model analogous to (6) to describe the turbulent motion of two compressible components. The model will take into account the turbulent motion of each component and the inertia motion due to the pulsation of the dispersed phase (bubbles). Since there is no ambiguity, the volume concentration of the dispersed component will be denoted by α instead of α_2.

In the general case, the following expression for the Lagrangian of the system can be given:

$$L = L\left(\boldsymbol{j}_1, \boldsymbol{j}_2, \bar{\rho}_1, \bar{\rho}_2, \mathscr{S}_1, \mathscr{S}_2, \mathscr{T}_1, \mathscr{T}_2, \alpha, \frac{\partial \alpha}{\partial t}, \nabla\alpha\right) \tag{9}$$

Here $\boldsymbol{j}_a = \bar{\rho}_a \boldsymbol{u}_a$ is the partial momentum of each component. The dependence of the Lagrangian on the derivatives of the volume concentration is due to the fact that we take into account the bubble pulsations. If the topology of the dispersed phase is prescribed (for example, a bubbly flow with bubbles having the same size), another parameters can be added such as, for example, the bubble number density. We do not consider the equation for this additional parameter, but it can be included without any difficulty. It changes some terms in the governing equations but conserves their mathematical structure. The variation of the Lagrangian (9) gives us the following governing equations (see Gavrilyuk & Saurel 2002 for details):

$$\frac{\partial \bar{\rho}_a}{\partial t} + \nabla\cdot(\bar{\rho}_a \boldsymbol{u}_a) = 0, \tag{10a}$$

$$\frac{\partial \mathscr{S}_a}{\partial t} + \nabla\cdot(\mathscr{S}_a \boldsymbol{u}_a) = 0, \quad \frac{\partial \mathscr{T}_a}{\partial t} + \nabla\cdot(\mathscr{T}_a \boldsymbol{u}_a) = 0, \tag{10b,c}$$

$$\bar{\rho}_a \frac{\partial \boldsymbol{K}_a}{\partial t} + \operatorname{rot} \boldsymbol{K}_a \wedge \boldsymbol{j}_a - \bar{\rho}_a \nabla\left(\frac{\partial L}{\partial \bar{\rho}_a}\right) - \mathscr{S}_a \nabla\left(\frac{\partial L}{\partial \mathscr{S}_a}\right) - \mathscr{T}_a \nabla\left(\frac{\partial L}{\partial \mathscr{T}_a}\right) = 0, \tag{10d}$$

$$\frac{\partial L}{\partial \alpha} - \frac{\partial}{\partial t}\left(\frac{\partial L}{\partial \alpha_t}\right) - \nabla\cdot\left(\frac{\partial L}{\partial \nabla\alpha}\right) = 0. \tag{10e}$$

Here $\boldsymbol{K}_a = \partial L / \partial \boldsymbol{j}_a$. Compared with the model developed in Gavrilyuk & Saurel (2002), new terms are added in the momentum equations:

$$-\mathscr{T}_a \nabla\left(\frac{\partial L}{\partial \mathscr{T}_a}\right).$$

They appear naturally via Hamilton's principle, because the turbulent 'entropies' $\mathscr{T}_a$ have the same status as the partial densities or the partial thermodynamic entropies. Equations (10) admit the conservation of the total momentum and the total energy. To present the equations in explicit form, the Lagrangian must be supplied.

3.1. *Explicit form of the Lagrangian*

Consider the following explicit form of the Lagrangian:

$$L = \sum_{a=1}^{2} \frac{|\boldsymbol{j}_a|^2}{2\bar{\rho}_a} + \frac{M}{2}\left(\frac{\mathrm{d}_I \alpha}{\mathrm{d}t}\right)^2 - \sum_{a=1}^{2}\left(\bar{\rho}_a e_a\left(\frac{\bar{\rho}_a}{\alpha_a}, \frac{\mathscr{S}_a}{\bar{\rho}_a}\right) + \mathscr{T}_a\left(\frac{\bar{\rho}_a}{\alpha_a}\right)^{\Gamma-1}\right). \tag{11}$$

Here the first term is the translational kinetic energy, the second is the kinetic energy due to the pulsations of the dispersed phase, and the two last terms are the internal energy and the turbulent energy of each component. We neglect the added mass effect (the dependence of the Lagrangian on the relative velocity) and denote

$$\frac{\mathrm{d}_I}{\mathrm{d}t} = \frac{\partial}{\partial t} + \boldsymbol{u}_I \cdot \nabla,$$

where the index 'I' means 'interface' $\boldsymbol{u}_I$ is the transport velocity of α (advection velocity of the interface between liquid and gas). The choice of $\boldsymbol{u}_I$ is crucial. When the continuous phase 1 is nearly incompressible, a good approximation is $\boldsymbol{u}_I = \boldsymbol{u}_1$, i.e. the interface is transported by the liquid phase. For the present application with two compressible fluids, this estimate can lead to some inaccuracies. Thus § 4 we will give other possible closure relations. The aim of the present section is to derive the governing equations without focusing on the closure issue. The various closure terms will be discussed in forthcoming sections.

The contribution of the pulsation energy is important when the compressibility of the dispersed phase is much higher than that of the continuous phase. Usually, if this is the case, we can suppose that

$$M = M(\alpha, \bar{\rho}_1). \tag{12}$$

For example, for bubbly fluid with a nearly incompressible liquid phase this energy can be written as $2\pi R^3 \rho_1 N(\mathrm{d}R/\mathrm{d}t)^2$, where R is the averaged bubble radius, $\rho_1 = \text{const}$ is the fluid density and N is the number of bubbles per unit volume (Lamb 1932). The volume concentration is given by the formula: $\alpha = \frac{4}{3}\pi R^3 N$. For the general case (12) we obtain the following governing equations (see Appendix A for the derivation):

$$\frac{\partial}{\partial t}\left(M\frac{\mathrm{d}_1\alpha}{\mathrm{d}t}\right) + \nabla\cdot\left(M\frac{\mathrm{d}_1\alpha}{\mathrm{d}t}\boldsymbol{u}_1\right) = P_2 - P_1 + \frac{1}{2}\frac{\partial M}{\partial \alpha}\left(\frac{\mathrm{d}_1\alpha}{\mathrm{d}t}\right)^2, \tag{13a}$$

$$\frac{\partial \alpha_1\rho_1}{\partial t} + \nabla\cdot(\alpha_1\rho_1\boldsymbol{u}_1) = 0, \quad \frac{\partial \alpha_2\rho_2}{\partial t} + \nabla\cdot(\alpha_2\rho_2\boldsymbol{u}_2) = 0, \tag{13b,c}$$

$$\frac{\partial \alpha_1\rho_1\boldsymbol{u}_1}{\partial t} + \nabla\cdot\left(\alpha_1\rho_1\boldsymbol{u}_1\otimes\boldsymbol{u}_1 + \left(\alpha_1 P_1 + \frac{1}{2}\left(M - \alpha_1\rho_1\frac{\partial M}{\partial \bar{\rho}_1}\right)\left(\frac{\mathrm{d}_1\alpha}{\mathrm{d}t}\right)^2\right)\boldsymbol{I}\right) = P_2\nabla\alpha_1, \tag{13d}$$

$$\frac{\partial \alpha_2\rho_2\boldsymbol{u}_2}{\partial t} + \nabla\cdot(\alpha_2\rho_2\boldsymbol{u}_2\otimes\boldsymbol{u}_2 + \alpha_2 P_2\boldsymbol{I}) = P_2\nabla\alpha_2, \tag{13e}$$

$$\frac{\partial}{\partial t}\left(\alpha_1\rho_1\left(\frac{|\boldsymbol{u}_1|^2}{2} + e_1 + \rho_1^{\Gamma-1}\varkappa_1\right) + \frac{M}{2}\left(\frac{\mathrm{d}_1\alpha}{\mathrm{d}t}\right)^2\right) + \nabla\cdot\left(\alpha_1\rho_1\boldsymbol{u}_1\left(\frac{|\boldsymbol{u}_1|^2}{2} + e_1 + \rho_1^{\Gamma-1}\varkappa_1\right)\right.$$
$$\left. + \boldsymbol{u}_1\left(M - \frac{\alpha_1\rho_1}{2}\frac{\partial M}{\partial \bar{\rho}_1}\right)\left(\frac{\mathrm{d}_1\alpha}{\mathrm{d}t}\right)^2 + \alpha_1\boldsymbol{u}_1 P_1\right) = -P_2\frac{\partial \alpha_1}{\partial t}, \tag{13f}$$

$$\frac{\partial}{\partial t}\left(\alpha_2\rho_2\left(\frac{|\boldsymbol{u}_2|^2}{2} + e_2 + \rho_2^{\Gamma-1}\varkappa_2\right)\right)$$
$$+ \nabla\cdot\left(\alpha_2\rho_2\boldsymbol{u}_2\left(\frac{|\boldsymbol{u}_2|^2}{2} + e_2 + \rho_2^{\Gamma-1}\varkappa_2\right) + \alpha_2\boldsymbol{u}_2 P_2\right) = -P_2\frac{\partial \alpha_2}{\partial t}, \tag{13g}$$

$$\frac{\partial \alpha_1\rho_1\varkappa_1}{\partial t} + \nabla\cdot(\alpha_1\rho_1\varkappa_1\boldsymbol{u}_1) = 0, \quad \frac{\partial \alpha_2\rho_2\varkappa_2}{\partial t} + \nabla\cdot(\alpha_2\rho_2\varkappa_2\boldsymbol{u}_2) = 0. \tag{13h,i}$$

We have denoted here by P_a the sum of the thermodynamic pressure and the turbulent pressure: $P_a = p_a + (\Gamma - 1)k_a$. In this model the interface pressure P_I is equal to the

pressure P_2 of the dispersed phase. The choice of the function M is important when inertia effects have to be taken into account. However, we know its expression only in the case of incompressible fluid. It is interesting to note that in the following two cases the Rayleigh–Lamb equation (13*a*) admits the useful representations:

$$\frac{\mathrm{d}_1\alpha}{\mathrm{d}t}=\frac{\tau\bar{\rho}_1}{\sqrt{m}},\quad \frac{\mathrm{d}_1\tau}{\mathrm{d}t}=\frac{P_2-P_1}{\bar{\rho}_1\sqrt{m}}\quad \text{if } M=m(\alpha), \tag{14}$$

$$\frac{\mathrm{d}_1\alpha}{\mathrm{d}t}=\frac{\tau}{\sqrt{m_1}},\quad \frac{\mathrm{d}_1\tau}{\mathrm{d}t}=\frac{P_2-P_1}{\bar{\rho}_1\sqrt{m_1}}\quad \text{if } M=\bar{\rho}_1 m_1(\alpha). \tag{15}$$

In this case the volume concentration α and the analogue of the interface radial velocity τ are the Riemann invariants changing along the velocity field $\boldsymbol{u}_1$(we have used here the same letter τ for different quantities). Case (14) was considered in Gavrilyuk & Saurel (2002) for the turbulence-free model.

3.2. *Dissipative system*

To deal with the general system of a two-phase mixture with internal degrees of freedom, dissipative effects have to be introduced in system (13). For simplicity, we present the dissipative system in case (15). The equations can be written in the form

$$\frac{\mathrm{d}_I\tau}{\mathrm{d}t}=\frac{P_2-P_1-P_\mu}{\alpha_1\rho_1\sqrt{m_1}},\quad \frac{\mathrm{d}_I\alpha}{\mathrm{d}t}=\frac{\tau}{\sqrt{m_1}},\quad \frac{\mathrm{d}_I}{\mathrm{d}t}=\frac{\partial}{\partial t}+\boldsymbol{u}_I\cdot\nabla,\quad \boldsymbol{u}_I=\boldsymbol{u}_1, \tag{16a–d}$$

$$\frac{\partial\alpha_1\rho_1}{\partial t}+\nabla\cdot(\alpha_1\rho_1\boldsymbol{u}_1)=0,\quad \frac{\partial\alpha_2\rho_2}{\partial t}+\nabla\cdot(\alpha_2\rho_2\boldsymbol{u}_2)=0, \tag{16e,f}$$

$$\frac{\partial\alpha_1\rho_1\boldsymbol{u}_1}{\partial t}+\nabla\cdot(\alpha_1\rho_1\boldsymbol{u}_1\otimes\boldsymbol{u}_1+\alpha_1P_1\boldsymbol{I})=P_I\nabla\alpha_1+\lambda(\boldsymbol{u}_2-\boldsymbol{u}_1),\quad P_I=P_2, \tag{16g,h}$$

$$\frac{\partial\alpha_2\rho_2\boldsymbol{u}_2}{\partial t}+\nabla\cdot(\alpha_2\rho_2\boldsymbol{u}_2\otimes\boldsymbol{u}_2+\alpha_2P_2\boldsymbol{I})=P_I\nabla\alpha_2-\lambda(\boldsymbol{u}_2-\boldsymbol{u}_1), \tag{16i}$$

$$\frac{\partial}{\partial t}\left(\alpha_1\rho_1\left(\frac{|\boldsymbol{u}_1|^2}{2}+e_1+\rho_1^{\Gamma-1}\varkappa_1+\frac{\tau^2}{2}\right)\right)+\nabla\cdot\left(\alpha_1\rho_1\boldsymbol{u}_1\left(\frac{|\boldsymbol{u}_1|^2}{2}+e_1+\rho_1^{\Gamma-1}\varkappa_1+\frac{\tau^2}{2}\right)+\alpha_1\boldsymbol{u}_1P_1\right)=-P_I\frac{\partial\alpha_1}{\partial t}+\lambda\boldsymbol{u}_I(\boldsymbol{u}_2-\boldsymbol{u}_1), \tag{16j}$$

$$\frac{\partial}{\partial t}\left(\alpha_2\rho_2\left(\frac{|\boldsymbol{u}_2|^2}{2}+e_2+\rho_2^{\Gamma-1}\varkappa_2\right)\right)+\nabla\cdot\left(\alpha_2\rho_2\boldsymbol{u}_2\left(\frac{|\boldsymbol{u}_2|^2}{2}+e_2+\rho_2^{\Gamma-1}\varkappa_2\right)+\alpha_2\boldsymbol{u}_2P_2\right)=-P_I\frac{\partial\alpha_2}{\partial t}-\lambda\boldsymbol{u}_I(\boldsymbol{u}_2-\boldsymbol{u}_2), \tag{16k}$$

$$\frac{\partial\alpha_1\rho_1\varkappa_1}{\partial t}+\nabla\cdot(\alpha_1\rho_1\varkappa_1\boldsymbol{u}_1)=\alpha_1\rho_1\dot{\varkappa}_1,\quad \frac{\partial\alpha_2\rho_2\varkappa_2}{\partial t}+\nabla\cdot(\alpha_2\rho_2\varkappa_2\boldsymbol{u}_2)=\alpha_2\rho_2\dot{\varkappa}_2. \tag{16l,m}$$

The term $\lambda(\boldsymbol{u}_2-\boldsymbol{u}_1)$ is the Stokes-type friction force, λ is a positive scalar function depending on the local parameters of the mixture and the relative velocity of the components, and P_μ is a viscous force which is responsible for the pulsation damping. In general, P_μ is proportional to τ: $P_\mu=\chi\tau$, $\chi>0$ (the analogue of the Stokes formula). Terms $\dot{\varkappa}_a$ represent the unknown production of turbulent entropy.

One can also prove that the energy equations are equivalent to

$$\left.\begin{aligned}\alpha_1\rho_1\theta_1\frac{\mathrm{d}_1\eta_1}{\mathrm{d}t}+\alpha_1\rho_1^{\Gamma}\dot{\varkappa}_1&=P_\mu\frac{\mathrm{d}_1\alpha}{\mathrm{d}t}\geqslant 0,\\ \alpha_2\rho_2\theta_2\frac{\mathrm{d}_2\eta_2}{\mathrm{d}t}+\alpha_2\rho_2^{\Gamma}\dot{\varkappa}_2&=\lambda\,(\boldsymbol{u}_2-\boldsymbol{u}_1)^2\geqslant 0.\end{aligned}\right\} \tag{17}$$

System (16) provides the general structure of a two-phase model involving two translational average velocities, one vibration velocity (pulsation of the dispersed phase) and internal rotation. The internal rotation is taken into account energetically as is usually done in turbulence modelling. Governing equations (16) have a 'classical' structure. However several modifications have been made. The equation for the volume concentration is given as a second-order equation. We have introduced the variable τ which is related to the pulsation velocity. This idea was also discussed in Bdzil *et al.* (1999), but the model was not presented in explicit form. Pressures P_1, P_2 and interface pressure P_I in momentum equations take into account the 'turbulence' pressure due to internal rotation. The 'turbulence' pressure difference is also responsible for the pulsations of the dispersed phase. The energy equations also contain the turbulence energy as well as the energy due to bubble pulsations.

This model has been tested for the case of shock wave propagation in bubbly fluid in the absence of internal rotation ($\varkappa_1 = 0, \varkappa_2 = 0$), and in the limit of very large drag coefficients ($\lambda \to +\infty$). An excellent agreement between numerical predictions and experimental measurements was obtained without using any adjustable parameters (Gavrilyuk & Saurel 2002). The proof of the hyperbolicity of the governing equations can be given in the same way as in the last reference.

3.3. *Baer–Nunziato-type model*

In many applications the internal inertia term can be neglected. This is possible when the compressibilities of the phases are not too different. In our application, with compressible fluids, inertia effects can be neglected, while internal rotation must be accounted for. Neglecting the micro-acceleration $\mathrm{d}_1\tau/\mathrm{d}t$ in the Rayleigh–Lamb equation, we obtain

$$P_2 - P_1 - P_\mu = 0.$$

Since $P_\mu = \chi\ \tau$, we have

$$\frac{\mathrm{d}_1\alpha}{\mathrm{d}t} = \frac{(P_2 - P_1)}{\chi\sqrt{m_1}}.$$

This equation replaces (16*a*, *b*). Moreover, if we also neglect the terms proportional to τ^2 in the equation of the energy balance for the first component (continuous phase), we obtain a generalization of the Baer–Nunziato (1986) model to the case of fluids with internal rotation (turbulence model):

$$\frac{\partial\alpha}{\partial t} + \boldsymbol{u}_I\cdot\nabla\alpha = \dot{\alpha} = \mu(P_2 - P_1), \quad \boldsymbol{u}_I = \boldsymbol{u}_1, \quad \alpha = \alpha_2, \tag{18a–c}$$

$$\frac{\partial\alpha_1\rho_1}{\partial t} + \nabla\cdot(\alpha_1\rho_1\boldsymbol{u}_1) = 0, \quad \frac{\partial\alpha_2\rho_2}{\partial t} + \nabla\cdot(\alpha_2\rho_2\boldsymbol{u}_2) = 0, \tag{18d, e}$$

$$\frac{\partial\alpha_1\rho_1\boldsymbol{u}_1}{\partial t} + \nabla\cdot(\alpha_1\rho_1\boldsymbol{u}_1\otimes\boldsymbol{u}_1 + \alpha_1 P_1\boldsymbol{I}) = P_I\nabla\alpha_1 + \lambda(\boldsymbol{u}_2 - \boldsymbol{u}_1), \quad P_I = P_2, \tag{18f, g}$$

$$\frac{\partial\alpha_2\rho_2\boldsymbol{u}_2}{\partial t} + \nabla\cdot(\alpha_2\rho_2\boldsymbol{u}_2\otimes\boldsymbol{u}_2 + \alpha_2 P_2\boldsymbol{I}) = P_I\nabla\alpha_2 - \lambda(\boldsymbol{u}_2 - \boldsymbol{u}_1), \tag{18h}$$

$$\frac{\partial}{\partial t}\left(\alpha_1\rho_1\left(\frac{|\boldsymbol{u}_1|^2}{2} + e_1 + \rho_1^{\Gamma-1}\varkappa_1\right)\right) + \nabla\cdot\left(\alpha_1\rho_1\boldsymbol{u}_1\left(\frac{|\boldsymbol{u}_1|^2}{2} + e_1 + \rho_1^{\Gamma-1}\varkappa_1\right) + \alpha_1\boldsymbol{u}_1 P_1\right) = -P_I\frac{\partial\alpha_1}{\partial t} + \lambda\boldsymbol{u}_I(\boldsymbol{u}_2 - \boldsymbol{u}_1), \tag{18i}$$

$$\frac{\partial}{\partial t}\left(\alpha_2\rho_2\left(\frac{|\boldsymbol{u}_2|^2}{2}+e_2+\rho_2^{\Gamma-1}\varkappa_2\right)\right)+\operatorname{div}\left(\alpha_2\rho_2\boldsymbol{u}_2\left(\frac{|\boldsymbol{u}_2|^2}{2}+e_2+\rho_2^{\Gamma-1}\varkappa_2\right)+\alpha_2\boldsymbol{u}_2P_2\right)$$
$$=-P_I\frac{\partial\alpha_2}{\partial t}-\lambda\boldsymbol{u}_I(\boldsymbol{u}_2-\boldsymbol{u}_2), \quad (18j)$$

$$\frac{\partial\alpha_1\rho_1\varkappa_1}{\partial t}+\nabla\cdot(\alpha_1\rho_1\varkappa_1\boldsymbol{u}_1)=\alpha_1\rho_1\dot{\varkappa}_1, \quad \frac{\partial\alpha_2\rho_2\varkappa_2}{\partial t}+\nabla\cdot(\alpha_2\rho_2\varkappa_2\boldsymbol{u}_2)=\alpha_2\rho_2\dot{\varkappa}_2. \quad (18k,l)$$

Here we denote $\mu=1/(\chi\sqrt{m_1})>0$. By summing the momentum equations and the energy equations, we obtain the conservation of the total momentum and the total energy.

In model (18) the interface pressure is equal to the pressure in the dispersed phase, and the interface velocity is equal to the velocity of the continuous phase. The fact that $P_I=P_2$ means that the pressure in the dispersed phase is nearly homogeneous. For other types of two-phase flows (for example, stratified flows) a different closure hypothesis could be used.

Models (16) and (18) contain several phenomenological parameters. For a bubbly flow some of them (λ and μ) can be found in terms of the viscosity coefficients and bubble sizes. In our application, the various fluids are compressible and non-dissipative, so that conventional closure relations cannot be used. For a gas bubble carried by another gas, it is necessary to find better approximations of P_I, $\boldsymbol{u}_I$ and to find appropriate relations for the 'drag' coefficient λ and pressure relaxation coefficient μ. The determination of the creation of turbulent entropy ($\dot{\varkappa}_1, \dot{\varkappa}_2$) during the interaction of a shock wave with a gas bubble is also crucial.

In the next Section we propose a different approach to the construction of multiphase flow models. Applying the new approach to a particular case of annular flows, we will obtain a model without adjustable parameters and presenting the same structure as model (18).

4. Discrete equation method (DEM)

The discrete equation method is a variant of averaging methods described, for example in Drew & Passman (1998). With conventional averaging method each pure fluid is governed by a continuum mechanics flow model that is selected and averaged with the help of a phase function. Such systems are usually non-conservative (this is also the case for equations (16), (18) obtained previously with the help of the Hamilton principle) and necessitate non-trivial closure relations. With these conventional approaches, the next step is to integrate numerically the PDE system over space and time. This poses a supplementary problem related to the numerical approximation of the non-conservative terms. An example of these difficulties is given in Hou & LeFloch (1994) and Dalmaso, LeFloch & Murat (1995), and a partial solution is given in Saurel & Abgrall (1999*a*).

With the discrete equation method we proceed in the opposite way to the usual one. The pure fluid equations are first integrated at the microscopic level, then the discrete formulae are averaged. This method is due to Abgrall & Saurel (2003) and has been developed for the numerical approximation of a seven-equation model (Baer & Nunziato 1986; Saurel & Abgrall 1999*a*; Saurel & LeMetayer 2001; Kapila *et al.* 2001). In these models, the microinertia effects are omitted. Also, the original DEM given in Abgrall & Saurel (2003) uses a probabilistic average of the discrete formulae to obtain the average model. Here, we use only geometrical averages to derive the model specific to the microstructure and topology of the flow under study.

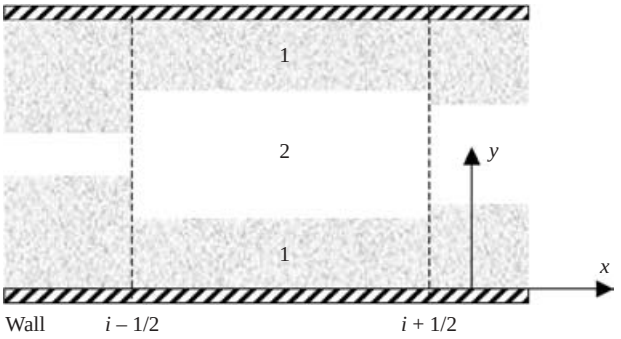

FIGURE 7. Schematic representation of a computational cell consisting of three horizontal fluid layers.

We summarize here the main ingredients of the DEM, and apply it to the k-model (6). We thus will solve the nine-equation model whose structure has been presented in the preceding Section. To be more precise, with the DEM the pure-phase conservation laws are considered at the microscopic level. They are integrated over space and time in the context of the interface problem at the microscale via the Godunov scheme (Godunov *et al.* 1979). These approximations are then averaged over the control volume and provide the corresponding numerical scheme for the averaged multiphase flow equations. The method provides the numerical scheme and contains implicitly the correct averages of the interfacial pressure and velocity as well as the relaxation terms. This will be proved in the next section by examining the continuous limit of the discrete equations.

The first step with the DEM is to define the topology of the two-phase mixture. In the particular case of a shock interaction with a light gas bubble, the bubble is assumed bigger than the one-dimensional control volume (the mesh size is smaller than the bubble size). Thus, in each computational cell, the two-phase flow is annular. The one-dimensional multiphase model is designed to save the computations of the other dimension. With minor modifications, the one-dimensional model would be applicable to two dimensions if the bubble was originally considered in three-dimensions.

We consider a computational mesh $x_i (i \in Z)$ and the associated control volumes $C_i =]x_{i-1/2}, x_{i+1/2}[\times]0, H[$ where $x_{i+1/2} = \frac{1}{2}(x_i + x_{i+1})$, and H represents the height of the tube section. The flow consists of two non-miscible phases 1 and 2. Since the bubble size is larger than the cell size, the two-phase mixture at the scale of the cell may be approximated by three horizontal layers separated by an interface as shown in figure 7. At the bubble extremities, this representation is still valid. The neighbouring cell will contain a negligible amount of gas.

Since this geometric configuration is two-dimensional, we must consider the two-dimensional conservation laws in each fluid. The fluids are assumed to be non-dissipative and rotation effects (turbulence effects) are to be considered in each fluid. Thus each pure fluid is governed by the two-dimensional k-model (6):

$$\frac{\partial \boldsymbol{W}}{\partial t} + \frac{\partial \boldsymbol{F}}{\partial x} + \frac{\partial \boldsymbol{G}}{\partial y} = 0 \tag{19}$$

with $\boldsymbol{W} = (1, \rho, \rho u, \rho v, \rho E, \rho \varkappa)^T$, $\boldsymbol{F} = (0, \rho u, \rho u^2 + p, \rho uv, (\rho E + P)u, \rho \varkappa u)^T$, $\boldsymbol{G} = (0, \rho v, \rho uv, \rho v^2 + p, (\rho E + P)v, \rho \varkappa v)^T$, the total energy is defined: $E = e + \frac{1}{2}(u^2 + v^2) + \rho^{\Gamma - 1} \varkappa$ and the same notation as previously is used. In equation (19), the k-model

has been supplemented by the identity

$$\frac{\partial 1}{\partial t}+\frac{\partial 0}{\partial x}+\frac{\partial 0}{\partial y}=0. \tag{20}$$

Equation (20) is used below in the presentation of the characteristic function equation.

The characteristic function X_a of the phase a ($X_a(t,x,y)=1$, if (x,y) belongs to fluid a at time t, and 0 otherwise), obeys the two-dimensional evolution equation:

$$\frac{\partial X_a}{\partial t}+\sigma_x\frac{\partial X_a}{\partial x}+\sigma_y\frac{\partial X_a}{\partial y}=0 \tag{21}$$

where σ_x and σ_y are the local interface velocity components (see, for example Drew & Passman 1998). Multiplying system (19) by the function X_a we obtain by using (21):

$$\frac{\partial X_a\boldsymbol{W}_a}{\partial t}+\frac{\partial X_a\boldsymbol{F}_a}{\partial x}+\frac{\partial X_a\boldsymbol{G}_a}{\partial y}=(\boldsymbol{F}_a-\sigma_x\boldsymbol{W}_a)\frac{\partial X_a}{\partial x}+(\boldsymbol{G}_a-\sigma_y\boldsymbol{W}_a)\frac{\partial X_a}{\partial y}. \tag{22}$$

This equation corresponds to the selection of the k-model in each fluid a. The first components of the conservative ($\boldsymbol{W}$) and flux ($\boldsymbol{F}$ and $\boldsymbol{G}$) vectors are those of equation (20). Thanks to identity (20), system (22) contains in a single formulation the characteristic function evolution equation (21) as well as the k-model for each phase. Integrating (22) over space and time, we obtain

$$\begin{aligned}&\int_0^{\Delta t}\int_{C_i}\left(\frac{\partial X_a\boldsymbol{W}_a}{\partial t}+\frac{\partial X_a\boldsymbol{F}_a}{\partial x}+\frac{\partial X_a\boldsymbol{G}_a}{\partial y}\right)\mathrm{d}x\,\mathrm{d}y\,\mathrm{d}s\\&=\int_0^{\Delta t}\int_{C_i}(\boldsymbol{F}_a-\sigma_x\boldsymbol{W}_a)\frac{\partial X_a}{\partial x}\,\mathrm{d}x\,\mathrm{d}y\,\mathrm{d}s+\int_0^{\Delta t}\int_{C_i}(\boldsymbol{G}_a-\sigma_y\boldsymbol{W}_a)\frac{\partial X_a}{\partial y}\,\mathrm{d}x\,\mathrm{d}y\,\mathrm{d}s\end{aligned} \tag{23}$$

Equation (23) is equivalent to

$$\boldsymbol{I}_1+\boldsymbol{I}_2+\boldsymbol{I}_3=\boldsymbol{I}_4+\boldsymbol{I}_5$$

with

$$\boldsymbol{I}_1=\int_0^{\Delta t}\int_{C_i}\frac{\partial X_a\boldsymbol{W}_a}{\partial t}\,\mathrm{d}x\,\mathrm{d}y\,\mathrm{d}s,\quad \boldsymbol{I}_2=\int_0^{\Delta t}\int_{C_i}\frac{\partial X_a\boldsymbol{F}_a}{\partial x}\,\mathrm{d}x\,\mathrm{d}y\,\mathrm{d}s,$$

$$\boldsymbol{I}_3=\int_0^{\Delta t}\int_{C_i}\frac{\partial X_a\boldsymbol{G}_a}{\partial y}\,\mathrm{d}x\,\mathrm{d}y\,\mathrm{d}s,\quad \boldsymbol{I}_4=\int_0^{\Delta t}\int_{C_i}\boldsymbol{F}_a^{lag}\frac{\partial X_a}{\partial x}\,\mathrm{d}x\,\mathrm{d}y\,\mathrm{d}s,$$

$$\boldsymbol{I}_5=\int_0^{\Delta t}\int_{C_i}\boldsymbol{G}_a^{lag}\frac{\partial X_a}{\partial y}\,\mathrm{d}x\,\mathrm{d}y\,\mathrm{d}s,$$

where $\boldsymbol{F}_a^{lag}=\boldsymbol{F}_a-\sigma_x\boldsymbol{W}_a$ and $\boldsymbol{G}_a^{lag}=\boldsymbol{G}_a-\sigma_y\boldsymbol{W}_a$ represent the Lagrangian fluxes. The numerical scheme consists of the approximation of these five integrals. These integrations are of paramount importance and are summarized in Appendix B.

Each integral $\boldsymbol{I}_1,\ldots,\boldsymbol{I}_5$ is now divided by $\Delta t\Delta x H$. The discretization of (23), for fluid 1 and for the geometrical description of the two-phase mixture in accordance with figure 7 is

$$\begin{aligned}&\frac{(\alpha\overline{\overline{\boldsymbol{W}}})_{1,i}^{n+1}-(\alpha\overline{\overline{\boldsymbol{W}}})_{1,i}^{n}}{\Delta t}+\frac{\langle\widetilde{X\boldsymbol{F}}\rangle_{1,i+1/2}-\langle\widetilde{X\boldsymbol{F}}\rangle_{1,i-1/2}}{\Delta x}\\&\qquad=\frac{\langle\widetilde{\boldsymbol{F}^{lag}}[X]\rangle_{1,i-1/2}+\langle\widetilde{\boldsymbol{F}^{lag}}[X]\rangle_{1,i+1/2}}{\Delta x}+\frac{\sum\{\widetilde{\boldsymbol{G}^{lag}}[X]\}_{1,i}}{H}.\end{aligned} \tag{24}$$

Here we have defined the following averaging operators. For any function f we define volume averages:

$$\overline{f} = \frac{1}{\Delta x H} \int_0^H \int_{-\Delta x/2}^{+\Delta x/2} f \, \mathrm{d}x \, \mathrm{d}y, \quad \overline{\overline{f}} = \frac{\overline{Xf}}{\overline{X}} = \frac{\overline{Xf}}{\alpha}, \tag{25}$$

and partial averages:

$$\begin{gathered} \langle f \rangle = \frac{1}{H} \int_0^H f \, \mathrm{d}y, \quad \widetilde{f} = \frac{1}{\Delta t} \int_0^{\Delta t} f \, \mathrm{d}t, \quad \{f\} = \frac{1}{\Delta x} \int_{-\Delta x/2}^{+\Delta x/2} f \, \mathrm{d}x, \\ \langle \widetilde{f} \rangle = \frac{1}{\Delta t H} \int_0^{\Delta t} \int_0^H f \, \mathrm{d}t \, \mathrm{d}y. \end{gathered} \tag{26}$$

In the last term of equation (24) symbol $\sum$ means summation over the horizontal interfaces.

The two-phase fluxes are (see Appendix B):

$$\begin{aligned} \langle \widetilde{X\boldsymbol{F}} \rangle_{1,i-1/2} &= X^*_{1,i-1/2}(1,2).\,\mathrm{Max}(0;\alpha_{1,i-1}-\alpha_{1,i})\boldsymbol{F}^*_{i-1/2}(1,2) \\ &\quad + X^*_{1,i-1/2}(1,1)\,\mathrm{Min}(\alpha_{1,i-1};\alpha_{1,i})\boldsymbol{F}^*_{i-1/2}(1,1) \\ &\quad + X^*_{1,i-1/2}(2,1)\,\mathrm{Max}(0;\alpha_{1,i}-\alpha_{1,i-1})\boldsymbol{F}^*_{i-1/2}(2,1), \\ \langle \widetilde{X\boldsymbol{F}} \rangle_{1,i+1/2} &= X^*_{1,i+1/2}(1,2).\,\mathrm{Max}(0;\alpha_{1,i}-\alpha_{1,i+1})\boldsymbol{F}^*_{i+1/2}(1,2) \\ &\quad + X^*_{1,i+1/2}(1,1)\,\mathrm{Min}(\alpha_{1,i+1};\alpha_{1,i})\boldsymbol{F}^*_{i+1/2}(1,1) \\ &\quad + X^*_{1,i+1/2}(2,1)\,\mathrm{Max}(0;\alpha_{1,i+1}-\alpha_{1,i})\boldsymbol{F}^*_{i+1/2}(2,1). \end{aligned}$$

And the non-conservative terms are (see Appendix B):

$$\begin{aligned} \langle \widetilde{\boldsymbol{F}^{lag}[X]} \rangle_{1,i-1/2} &= [X^*_1]_{i-1/2}(1,2)\,\mathrm{Max}(0;\alpha_{1,i-1}-\alpha_{1,i})\boldsymbol{F}^{lag,*}_{i-1/2}(1,2) \\ &\quad + [X^*_1]_{i-1/2}(2,1)\,\mathrm{Max}(0;\alpha_{1,i}-\alpha_{1,i-1})\boldsymbol{F}^{lag,*}_{i-1/2}(2,1), \\ \langle \widetilde{\boldsymbol{F}^{lag}[X]} \rangle_{1,i+1/2} &= [X^*_1]_{i+1/2}(1,2)\,\mathrm{Max}(0;\alpha_{1,i}-\alpha_{1,i+1})\boldsymbol{F}^{lag,*}_{i+1/2}(1,2) \\ &\quad + [X^*_1]_{i+1/2}(2,1)\,\mathrm{Max}(0;\alpha_{1,i+1}-\alpha_{1,i})\boldsymbol{F}^{lag,*}_{i+1/2}(2,1), \end{aligned}$$

$$\sum \{\widetilde{\boldsymbol{G}^{lag}[X]}\}_{1,i} = \boldsymbol{G}^{lag,*}(2,1) - \boldsymbol{G}^{lag,*}(1,2).$$

In these formulae, the notation (p,q) denotes a flow pattern such that fluid p is on the left and q on the right (see Appendix B for details) and the superscript * means the solution of the Riemann problem.

System (24) is a discrete analogue of system (18). To show that the mathematical structure of the discrete model (24) and the continuous one (18) are the same it is necessary to determine the continuous limit of the discrete equations. To do this, we need an approximate Riemann solver.

5. Riemann solver

The Eulerian and Lagrangian fluxes as well as the contact wave speed in equation (24) are determined by solving the one-dimensional Riemann problem for the k-model (6):

$$\frac{\partial \boldsymbol{W}}{\partial t} + \frac{\partial \boldsymbol{F}}{\partial x} = 0 \tag{27}$$

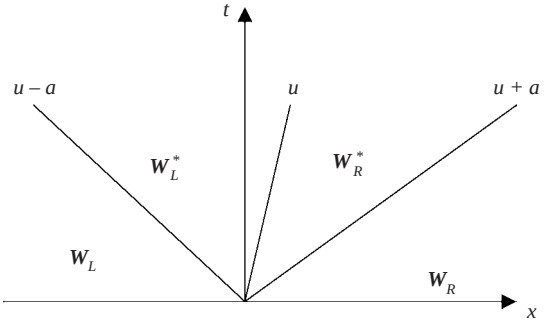

FIGURE 8. Schematic representation of the linearized Riemann problem solution.

with $\boldsymbol{W}=(\rho, \rho u, \rho E, \rho\varkappa)^T$, $\boldsymbol{F}=(\rho u, \rho u^2+P, (\rho E+P)u, \rho\varkappa u)^T$ and the same notation as previously. This system has the following eigenvalues:

(i) a double eigenvalue corresponding to the contact discontinuity: $\lambda_{1,2}=u$;

(ii) two distinct eigenvalues corresponding to the left and right facing acoustic waves, respectively: $\lambda_3=u-a$ and $\lambda_4=u+a$.

The 'turbulent' speed of sound a is $a^2=c^2+\Gamma(\Gamma-1)\rho^{\Gamma-1}\varkappa$. The thermodynamic speed of sound c is obtained from the equation of state:

$$\rho c^2=\frac{\dfrac{p}{\rho}-\rho\left(\dfrac{\partial e}{\partial\rho}\right)_p}{\left(\dfrac{\partial e}{\partial p}\right)_\rho}.$$

The characteristic system is

$$\left.\begin{aligned}
&\frac{\mathrm{d}P}{\mathrm{d}t}+\rho a\frac{\mathrm{d}u}{\mathrm{d}t}=0 \quad \text{along} \quad \frac{\mathrm{d}x}{\mathrm{d}t}=u+a,\\
&\frac{\mathrm{d}P}{\mathrm{d}t}-\rho a\frac{\mathrm{d}u}{\mathrm{d}t}=0 \quad \text{along} \quad \frac{\mathrm{d}x}{\mathrm{d}t}=u-a,\\
&\frac{\mathrm{d}\varkappa}{\mathrm{d}t}=0 \quad \text{along} \quad \frac{\mathrm{d}x}{\mathrm{d}t}=u,\\
&\frac{\mathrm{d}P}{\mathrm{d}t}-a^2\frac{\mathrm{d}\rho}{\mathrm{d}t}=0 \quad \text{along} \quad \frac{\mathrm{d}x}{\mathrm{d}t}=u.
\end{aligned}\right\} \tag{28}$$

It is also easy to express the Riemann invariants across the contact wave $\lambda_{1,2}=u$. They are also the Rankine–Hugoniot conditions at the contact discontinuity: $[\boldsymbol{F}-u\boldsymbol{W}]=\boldsymbol{0}$. This relation yields the following interface conditions: $[P]=0$ and $[u]=0$. These interface conditions are particularly important for our application. They express the fact that a local depression, separating two media having different turbulent entropies, will be convected at the contact discontinuity velocity.

To derive an approximate Riemann solver for the k-model, we adopt the procedure described in Toro (1997) in the context of Euler equations. This procedure is called the 'acoustic approximate Riemann solver'. This solver is able to deal with real materials and complicated equations of state, and it is fast and robust enough for most applications.

The Riemann problem is solved between the left-state $\boldsymbol{W}_L$ and the right-state $\boldsymbol{W}_R$ as shown in figure 8. We denote the acoustic impedance by $Z=\rho a$ where a is the

turbulent sound speed. The linearized solution of the Riemann problem is

$$\left.\begin{aligned} P^* &= \frac{Z_R P_L + Z_L P_R + Z_L Z_R (u_L - u_R)}{Z_L + Z_R}, \\ u^* &= \frac{Z_L u_L + Z_R u_R + (P_L - P_R)}{Z_L + Z_R}, \\ \rho_L^* &= \rho_L + (P^* - P_L)/a_L^2, \quad \rho_R^* = \rho_R + (P^* - P_R)/a_R^2, \\ \varkappa_L^* &= \varkappa_L, \quad \varkappa_R^* = \varkappa_R, \end{aligned}\right\} \tag{29}$$

where the asterisk designates the state corresponding to the contact discontinuity.

6. Continuous limit of the discrete equations

The aim of this Section is to show that the discrete equations contain implicitly the relaxation terms as well as the expressions for the averaged interfacial pressure and velocity. Knowledge of the continuous limit can also be helpful for a better understanding of the model structure. The continuous limit of the discrete equations consists of determining the system of partial differential equations resulting from equation (24) when both $\Delta t \to 0$ and $\Delta x \to 0$. In this limit, some averages defined by (25) and (26) are simplified:

$$\overline{\overline{f}} \to \langle f \rangle, \quad \langle \tilde{f} \rangle \to \langle f \rangle, \quad \{f\} \to f.$$

Thus equation (24) becomes

$$\frac{(\alpha \langle \boldsymbol{W} \rangle)_{1,i}^{n+1} - (\alpha \langle \boldsymbol{W} \rangle)_{1,i}^{n}}{\Delta t} + \frac{\langle X \boldsymbol{F} \rangle_{1,i+1/2} - \langle X \boldsymbol{F} \rangle_{1,i-1/2}}{\Delta x} = \frac{\langle \boldsymbol{F}^{lag}[X] \rangle_{1,i-1/2} + \langle \boldsymbol{F}^{lag}[X] \rangle_{1,i+1/2}}{\Delta x} + \frac{\boldsymbol{G}_{1,i}^{lag,*}(2,1) - \boldsymbol{G}_{1,i}^{lag,*}(1,2)}{H}.$$

To simplify the notation, we omit subscript 1 in the following. Four terms are to be examined.

6.1. *Temporal term*

The continuous limit of the temporal term does not present any difficulty:

$$\frac{(\alpha \langle \boldsymbol{W} \rangle)_i^{n+1} - (\alpha \langle \boldsymbol{W} \rangle)_i^{n}}{\Delta t} \to \frac{\partial \alpha \langle \boldsymbol{W} \rangle}{\partial t}.$$

6.2. *Fluxes*

Analogously, the continuous limit of the fluxes is

$$\frac{\langle X \boldsymbol{F} \rangle_{i+1/2} - \langle X \boldsymbol{F} \rangle_{i-1/2}}{\Delta x} \to \frac{\partial \langle X \boldsymbol{F} \rangle}{\partial x} = \frac{\partial \alpha \langle \boldsymbol{F} \rangle}{\partial x}.$$

6.3. *Non-conservative terms*

We now determine the limit of the following term:

$$\langle \boldsymbol{F}^{lag}[X] \rangle_{i-1/2} + \langle \boldsymbol{F}^{lag}[X] \rangle_{i+1/2} = \begin{pmatrix} [X^*]_{i-1/2}(1,2)\,\mathrm{Max}(0; \alpha_{i-1} - \alpha_i)\boldsymbol{F}_{i-1/2}^{lag,*}(1,2) \\ + [X^*]_{i-1/2}(2,1)\,\mathrm{Max}(0; \alpha_i - \alpha_{i-1})\boldsymbol{F}_{i-1/2}^{lag,*}(2,1) \\ + [X^*]_{i+1/2}(1,2)\,\mathrm{Max}(0; \alpha_i - \alpha_{i+1})\boldsymbol{F}_{i+1/2}^{lag,*}(1,2) \\ + [X^*]_{i+1/2}(2,1)\,\mathrm{Max}(0; \alpha_{i+1} - \alpha_i)\boldsymbol{F}_{i+1/2}^{lag,*}(2,1) \end{pmatrix}.$$

To facilitate the calculations we introduce for any function f the following notation:

$$f^+ = \mathrm{Max}(0, f) = \frac{f + |f|}{2},$$

$$f^- = \mathrm{Min}(0, f) = \frac{f - |f|}{2}.$$

Let $\delta\alpha = \alpha_i - \alpha_{i-1}$. Then

$$\mathrm{Max}(0; \alpha_{i-1} - \alpha_i) = Max(0, -\delta\alpha) = -\delta\alpha^-,$$

$$\mathrm{Min}(\alpha_{i-1}, \alpha_i) = \frac{\alpha_{i-1}\delta\alpha^+ - \alpha_i\delta\alpha^-}{|\delta\alpha|},$$

$$\mathrm{Max}(0; \alpha_i - \alpha_{i-1}) = Max(0, \delta\alpha) = \delta\alpha^+.$$

The jumps of the indicator function X^* are given in Appendix B (table 2). With these definitions the non-conservative term is

$$\langle \boldsymbol{F}^{lag}[X]\rangle_{i-1/2} + \langle \boldsymbol{F}^{lag}[X]\rangle_{i+1/2} = \begin{pmatrix} \left(\dfrac{u^{*,+}}{|u^*|}\right)_{i-1/2}(1,2)\delta\alpha^-_{i-1/2}\boldsymbol{F}^{lag,*}_{i-1/2}(1,2) \\ +\left(\dfrac{u^{*,+}}{|u^*|}\right)_{i-1/2}(2,1)\delta\alpha^+_{i-1/2}\boldsymbol{F}^{lag,*}_{i-1/2}(2,1) \\ -\left(\dfrac{u^{*,-}}{|u^*|}\right)_{i+1/2}(1,2)\delta\alpha^-_{i+1/2}\boldsymbol{F}^{lag,*}_{i+1/2}(1,2) \\ -\left(\dfrac{u^{*,-}}{|u^*|}\right)_{i+1/2}(2,1)\delta\alpha^+_{i+1/2}\boldsymbol{F}^{lag,*}_{i+1/2}(2,1) \end{pmatrix}.$$

Under the assumption that the solution in each pure fluid is continuous we find in the limit when $\Delta x \to 0$: $u^*_{i-1/2}(1,2) = u^*_{i+1/2}(1,2) = u^*(1,2)$ and $u^*_{i-1/2}(2,1) = u^*_{i+1/2}(2,1) = u^*(2,1)$ as well as $\boldsymbol{F}^{lag,*}_{i-1/2}(1,2) = \boldsymbol{F}^{lag,*}_{i+1/2}(1,2) = \boldsymbol{F}^{lag,*}(1,2)$ and $\boldsymbol{F}^{lag,*}_{i-1/2}(2,1) = \boldsymbol{F}^{lag,*}_{i+1/2}(2,1) = \boldsymbol{F}^{lag,*}(2,1)$. Thus, the preceding non-conservative term reduces to

$$\langle \boldsymbol{F}^{lag}[X]\rangle_{i-1/2} + \langle \boldsymbol{F}^{lag}[X]\rangle_{i+1/2} = \delta\alpha^-\boldsymbol{F}^{lag,*}(1,2) + \delta\alpha^+\boldsymbol{F}^{lag,*}(2,1).$$

The Lagrangian flux $\boldsymbol{F}^{lag} = (-u, 0, P, 0, Pu, 0)^T$. Thus, only three components are non-trivial.

Volume fraction equation

For the first equation of system (24) the associated first component of $\boldsymbol{F}^{lag}$ is

$$(\boldsymbol{F}^{lag}(p,q))^1 = -u^*(p,q)$$

Thus the non-conservative term becomes

$$\left(\frac{\langle \boldsymbol{F}^{lag}[X]\rangle_{i-1/2} + \langle \boldsymbol{F}^{lag}[X]\rangle_{i+1/2}}{\Delta x}\right)^1 = -\left(\frac{\delta\alpha^-}{\Delta x}u^*(1,2) + \frac{\delta\alpha^+}{\Delta x}u^*(2,1)\right)^1.$$

The Riemann solver gives

$$u^*(1,2) = \frac{Z_1u_1 + Z_2u_2}{Z_1 + Z_2} + \frac{P_1 - P_2}{Z_1 + Z_2}$$

and

$$u^*(2,1) = \frac{Z_1u_1 + Z_2u_2}{Z_1 + Z_2} + \frac{P_2 - P_1}{Z_1 + Z_2}.$$

Thus the non-conservative term can be written as

$$\left(\frac{\langle \boldsymbol{F}^{lag}[X]\rangle_{i-1/2} + \langle \boldsymbol{F}^{lag}[X]\rangle_{i+1/2}}{\Delta x}\right)^1 = -\frac{\delta\alpha}{\Delta x} u_I$$

where u_I is given by

$$u_I = \frac{Z_1 u_1 + Z_2 u_2}{Z_1 + Z_2} + \operatorname{sgn}\left(\frac{\partial\alpha}{\partial x}\right)\frac{P_2 - P_1}{Z_1 + Z_2} \tag{30}$$

In the limit we obtain

$$\left(\frac{\langle \boldsymbol{F}^{lag}[X]\rangle_{i-1/2} + \langle \boldsymbol{F}^{lag}[X]\rangle_{i+1/2}}{\Delta x}\right)^1 = -u_I \frac{\partial\alpha}{\partial x}.$$

Momentum equation

For the third equation of system (24) the associated component of $\boldsymbol{F}^{lag}$ is

$$(\boldsymbol{F}^{lag}(p,q))^3 = P^*(p,q).$$

Thus the non-conservative term becomes

$$\left(\frac{\langle \boldsymbol{F}^{lag}[X]\rangle_{i-1/2} + \langle \boldsymbol{F}^{lag}[X]\rangle_{i+1/2}}{\Delta x}\right)^3 = \left(\frac{\delta\alpha^-}{\Delta x} P^*(1,2) + \frac{\delta\alpha^+}{\Delta x} P^*(2,1)\right)^3.$$

Using the same arguments as previously, it reduces to

$$\left(\frac{\langle \boldsymbol{F}^{lag}[X]\rangle_{i-1/2} + \langle \boldsymbol{F}^{lag}[X]\rangle_{i+1/2}}{\Delta x}\right)^3 = \frac{\delta\alpha}{\Delta x} P_I$$

where the interface pressure is

$$P_I = \frac{Z_1 P_2 + Z_2 P_1}{Z_1 + Z_2} + \operatorname{sgn}\left(\frac{\partial\alpha}{\partial x}\right)\frac{(u_2 - u_1) Z_1 Z_2}{Z_1 + Z_2} \tag{31}$$

In the limit we have

$$\left(\frac{\langle \boldsymbol{F}^{lag}[X]\rangle_{i-1/2} + \langle \boldsymbol{F}^{lag}[X]\rangle_{i+1/2}}{\Delta x}\right)^3 = P_I \frac{\partial\alpha}{\partial x}.$$

Energy equation

From the same analysis we obtain

$$\left(\frac{\langle \boldsymbol{F}^{lag}[X]\rangle_{i-1/2} + \langle \boldsymbol{F}^{lag}[X]\rangle_{i+1/2}}{\Delta x}\right)^5 = P_I u_I \frac{\partial\alpha}{\partial x}.$$

6.4. *Relaxation terms*

For the annular flow the relaxation terms associated with the presence of horizontal interfaces are

$$\frac{\boldsymbol{G}^{lag,*}_{1,i}(2,1) - \boldsymbol{G}^{lag,*}_{1,i}(1,2)}{H}.$$

Since the Lagrangian flux is $\boldsymbol{G}^{lag} = (-v, 0, 0, P, Pv, 0)^T$, only three components are non-zero.

Volume fraction variations

The first non-zero term is

$$\left(\frac{\boldsymbol{G}^{lag,*}_{1,i}(2,1) - \boldsymbol{G}^{lag,*}_{1,i}(1,2)}{H}\right)^1 = \frac{1}{H}(-v^*(2,1) + v^*(1,2)).$$

By using formulae (29) where we replace the horizontal velocity u by the vertical velocity v, we obtain

$$-v^*(2,1)+v^*(1,2)=\frac{2(P_1-P_2)}{Z_1+Z_2}$$

which expresses the rate of change of volume fraction α_1 of fluid 1 due to the pressure relaxation:

$$\dot{\alpha_1}=\frac{2(P_1-P_2)}{H(Z_1+Z_2)}.$$

Consequently, the pressure relaxation coefficient introduced in system (18) is

$$\mu=\frac{2}{H(Z_1+Z_2)}. \tag{32}$$

Momentum relaxation

We now examine the second non-zero term of the non-conservative vector:

$$\left(\frac{\boldsymbol{G}_{1,i}^{lag,*}(2,1)-\boldsymbol{G}_{1,i}^{lag,*}(1,2)}{H}\right)^4=\frac{1}{H}(P^*(2,1)-P^*(1,2)).$$

By using formulae (29) with $v_L=v_R=0$ we obtain

$$P^*(2,1)-P^*(1,2),$$

indicating that the vertical velocity will remain zero, and that there is no contribution to the drag force due to horizontal interfaces. This is not surprising, since the horizontal interfaces are slip lines for the fluids flowing in the x-direction. Thus, the velocity relaxation coefficient (drag coefficient) is zero:

$$\lambda=0.$$

This is in agreement with the fact that the fluids are inviscid. But it does not mean that the velocities of the fluids evolve without interactions. The interface pressure (31) with the non-conservative term of the x-momentum component involves a velocity difference, implying velocity relaxation.

Energy variation due to pressure relaxation

The last step consists of the evaluation of the pressure work due to the fifth non-zero component of the non-conservative vector

$$\left(\frac{\boldsymbol{G}_{1,i}^{lag,*}(2,1)-\boldsymbol{G}_{1,i}^{lag,*}(1,2)}{H}\right)^5=\frac{1}{H}((Pv)^*(2,1)-(Pv)^*(1,2)).$$

Using again the Riemann solver it follows that

$$(Pv)^*(2,1)-(Pv)^*(1,2)=-\frac{Z_2P_1+Z_1P_2}{Z_1+Z_2}\frac{2(P_1-P_2)}{Z_1+Z_2}.$$

This can be written

$$P_I^{'}\dot{\alpha_1}=\frac{Z_2P_1+Z_1P_2}{Z_1+Z_2}\frac{2(P_1-P_2)}{H(Z_1+Z_2)}$$

Here the volume fraction variation rate is recovered with a different interface pressure

$$P_I^{'}=\frac{Z_2P_1+Z_1P_2}{Z_1+Z_2}$$

associated with interface vertical motion. This formula is a particular case of (31) when the fluid vertical velocities are zero.

6.5. *Summary of the continuous limit of the discrete equations*

We present the one-dimensional system only for fluid 1, the system being symmetric for fluid 2. Omitting the averaging operator we obtain the following limit system:

$$\frac{\partial \alpha_1}{\partial t} + u_I \frac{\partial \alpha_1}{\partial x} = \mu(P_1 - P_2), \tag{33a}$$

$$\frac{\partial \alpha_1 \rho_1}{\partial t} + \frac{\partial(\alpha_1 \rho_1 u_1)}{\partial x} = 0, \tag{33b}$$

$$\frac{\partial \alpha_1 \rho_1 u_1}{\partial t} + \frac{\partial(\alpha_1 \rho_1 u_1^2 + \alpha_1 P_1)}{\partial x} = P_I \frac{\partial \alpha_1}{\partial x}, \tag{33c}$$

$$\frac{\partial \alpha_1 \rho_1 E_1}{\partial t} + \frac{\partial(\alpha_1 \rho_1 E_1 u_1 + \alpha_1 P_1 u_1)}{\partial x} = P_I u_I \frac{\partial \alpha_1}{\partial x} - \mu P_I'(P_1 - P_2), \tag{33d}$$

$$\frac{\partial \alpha_1 \rho_1 \varkappa_1}{\partial t} + \frac{\partial(\alpha_1 \rho_1 \varkappa_1 u_1)}{\partial x} = \alpha_1 \rho_1 \dot{\varkappa}_1, \tag{33e}$$

with

$$P_I = \frac{Z_1 P_2 + Z_2 P_1}{Z_1 + Z_2} + \operatorname{sgn}\left(\frac{\partial \alpha_1}{\partial x}\right) \frac{(u_2 - u_1) Z_1 Z_2}{Z_1 + Z_2}, \quad P_I' = \frac{Z_1 P_2 + Z_2 P_1}{Z_1 + Z_2},$$

$$u_I = \frac{Z_1 u_1 + Z_2 u_2}{Z_1 + Z_2} + \operatorname{sgn}\left(\frac{\partial \alpha_1}{\partial x}\right) \frac{P_2 - P_1}{Z_1 + Z_2}, \quad \mu = \frac{2}{H(Z_2 + Z_1)}.$$

The continuous limit of the discrete equations demonstrates that the full discrete equations contain intrinsically the relaxation terms and the averages of interfacial variables.

The structure of this system is very close to (18), where we have to put one of the relaxation parameters equal to zero ($\lambda = 0$). The only difference is the term $\mu P_I'(P_1 - P_2)$ instead of $\mu P_I(P_1 - P_2)$ as in (18). However, in the limit when the acoustic impedances are very different ($Z_1 \gg Z_2$) systems (18) and (33) have the same interface pressure and velocity, with explicit expressions for relaxation parameters.

7. Turbulence production

To determine the turbulence production term $\dot{\varkappa}_1$ we analyse the total entropy creation in each fluid. As a consequence of (33), we obtain the following identity for fluid 1:

$$\alpha_1 \rho_1 \theta_1 \frac{\mathrm{d}_1 \eta_1}{\mathrm{d}t} + \alpha_1 \rho_1^{\Gamma} \frac{\mathrm{d}_1 \varkappa_1}{\mathrm{d}t} = (P_I - P_1)(u_I - u_1) \frac{\partial \alpha_1}{\partial x} - (P_I' - P_1)\mu(P_1 - P_2). \tag{34}$$

Replacing the expressions for u_I, P_I and P_I' we obtain the inequality analogous to (17):

$$\alpha_1 \rho_1 \theta_1 \frac{\mathrm{d}_1 \eta_1}{\mathrm{d}t} + \alpha_1 \rho_1^{\Gamma} \frac{\mathrm{d}_1 \varkappa_1}{\mathrm{d}t} = \frac{Z_1}{(Z_1 + Z_2)^2} \left(\left((P_2 - P_1) + \operatorname{sgn}\left(\frac{\partial \alpha_1}{\partial x}\right)(u_2 - u_1) Z_2 \right)^2 \left| \frac{\partial \alpha_1}{\partial x} \right| + \frac{2}{H}(P_2 - P_1)^2 \right) \geqslant 0.$$

Now we assume that:

(i) During the shock propagation in each pure fluid the thermodynamic entropy increases as is usually the case. This is accounted for by the fact that the Rankine–Hugoniot conditions are fulfilled in each fluid and are responsible for the increase of the thermodynamic entropy.

(ii) After the shock wave interaction with the bubble, the thermodynamic entropy does not change. In other words, the entropy creation after the shock propagation is stored by the largest flow structures (the bubbles) in the form of turbulent entropy.

(iii) The time scale is such that the further transfer of the turbulent entropy to the thermodynamic entropy is negligible.

This permits us to write directly the equation for the turbulent entropy creation:

$$\dot{\varkappa}_1 = \frac{Z_1}{\alpha_1 \rho_1^{\Gamma} (Z_1 + Z_2)^2} \left(\left((P_2 - P_1) + \operatorname{sgn} \left(\frac{\partial \alpha_1}{\partial x} \right) (u_2 - u_1) Z_2 \right)^2 \left| \frac{\partial \alpha_1}{\partial x} \right| + \frac{2}{H} (P_2 - P_1)^2 \right). \tag{35}$$

We note that all the right-hand sides are computed without any adjustable parameters. The only assumptions are:

(*a*) The two-phase flow is annular.

(*b*) One-dimensional Riemann solvers are used for the various fluxes calculations.

(*c*) There is no thermodynamic entropy creation during rotation production after the shock wave propagation. This is a consequence of the fact that no heat exchange and no dissipation is present in each pure fluid since the phenomenon considered is very fast.

(*d*) The multi-valued character of the interface velocity and of most flow variables are not considered.

For the present application these assumptions are not too restrictive. The only real hypotheses are (*a*) and (*d*) and this will be the subject of future investigations. We now examine the validity of the model.

8. Test problems

We now examine the accuracy of the model for two test problems. The first one does not involve any rotation or turbulence. It is a liquid–gas shock tube where we examine the ability of the model to fulfil the interface conditions. The liquid chamber is separated from the gas chamber by a liquid–gas interface. The aim of this test is to show that the model is able to solve automatically interface problems between pure (or nearly pure) fluids. Second, we examine the model behaviour for the two-dimensional shock–bubble interaction test problem (figure 1).

Water–air shock tube

We consider a shock tube filled on the left-hand side with high-pressure water and on the right-hand side with air. This test problem consists of a conventional shock tube with two fluids and possesses an exact solution. For this test problem, standard numerical methods based on the Euler equations resolution fail at the second time step.

Each fluid is governed by the stiffened gas equation of state:

$$p = (\gamma - 1)\rho e - \gamma p_{\infty} \tag{36}$$

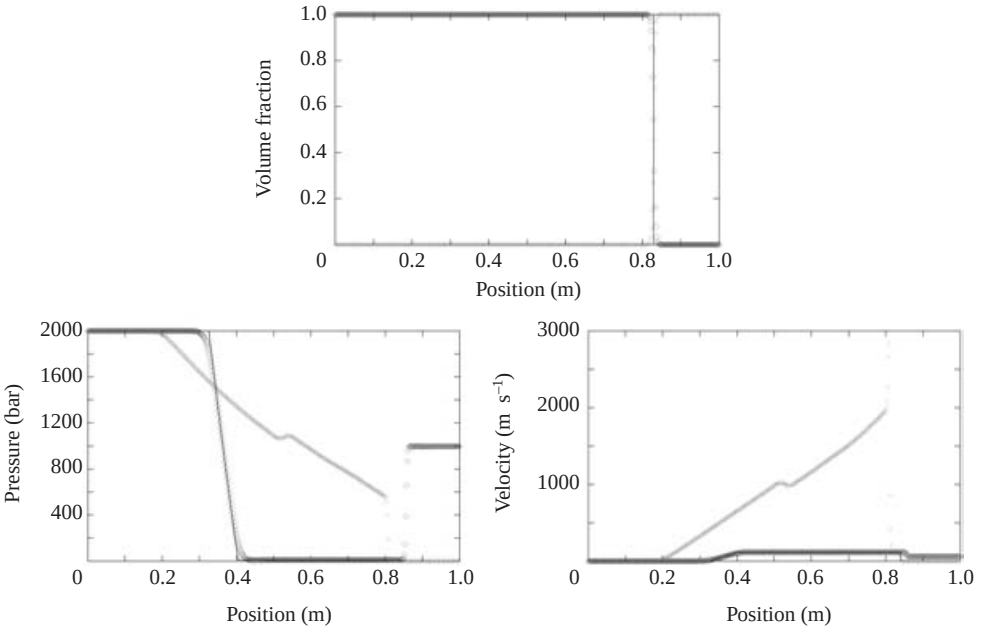

FIGURE 9. Test problem of a shock tube with interface separating nearly pure materials. The second-order scheme is used. Exact solution is shown with lines, numerical solution with symbols. Each fluid has a different behaviour, but at the interface, the pressures and velocities become equal.

where γ and p_∞ are constant parameters. The initial data are: $\rho_l = 1000\,\mathrm{kg\,m^{-3}}$, $p_l = 10^9\,\mathrm{Pa}$, $u_l = 0\,\mathrm{m\,s^{-1}}$, $\gamma_l = 4.4$, $p_{\infty_l} = 6.10^8\,\mathrm{Pa}$, $\alpha_l = 1 - \epsilon(\epsilon = 10^{-6})$ if $x < 0.7$; $\rho_g = 50\,\mathrm{kg\,m^{-3}}$, $p_g = 10^5\,\mathrm{Pa}$, $u_g = 0\,\mathrm{m\,s^{-1}}$, $\gamma_g = 1.4$, $p_{\infty_g} = 0$, $\alpha_g = 1 - \epsilon$ otherwise.

To show the mesh convergence of the results, a mesh involving 1000 cells is used. The corresponding results are shown in figure 9 at time 229 ms. In this test case, the right- and left-hand chambers contain nearly pure fluids: the volume fraction of gas in the water chamber is only 10^{-6} and inversely in the gas chamber. The phases densities and internal energies are not compared with the exact solution because no exact solution exists for these variables (no exact Riemann solver is available for this model). But the mixture density, the phase pressures and velocities can be compared with the exact solution. We now use the scheme (24) with the second-order extension described in Abgrall & Saurel (2003). Also, the transverse non-conservative terms are removed: $\sum\{\boldsymbol{G}^{lag}[X]\} = 0$ in order to not account for any two-dimensional pressure relaxation effect.

Results are shown in figure 9. It can be noticed that the two fluids have very different pressure and velocity profiles. In the left part of this shock tube, the liquid is nearly pure and fits perfectly the exact solution. The gas phase has different behaviour due to its different equation of state. We can also notice that the gas phase accelerates near the interface. This is due to space and time variations of the volume fraction inside the numerical diffusion zone of the interface. Since the gas evolves in a very small volume (initial volume fraction of 10^{-6}), slight variations in volume fraction induce large effects. But the most interesting fact is that the interface conditions are perfectly matched. In the right part, the shock tube contains a nearly pure gas. Its velocity is automatically adjusted to that of the liquid in the left chamber. A magnified view of these variables is shown in figure 10.

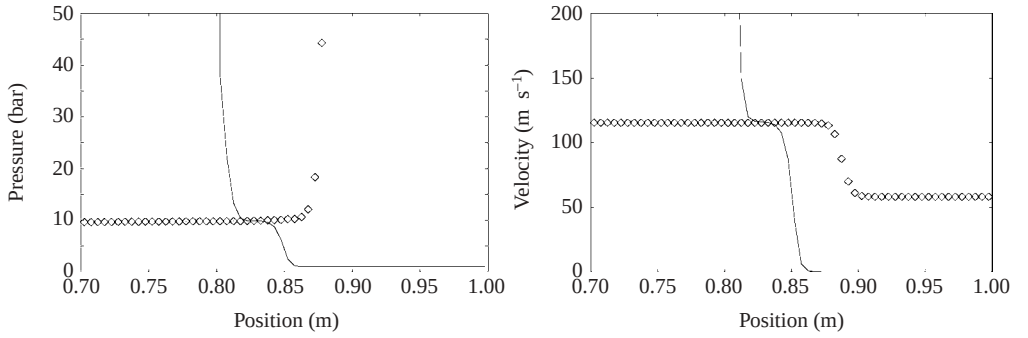

FIGURE 10. Magnified view of the pressure and velocity profiles near the interface for the test in figure 9. The liquid is shown with diamond symbols. The gas shown with lines. The interface conditions are automatically fulfilled.

This method has a very nice feature. It is able to deal with non-equilibrium mixtures as well as with interface problems. This is important for the fulfilment of interface conditions at the bubble edge considered in the next test problem. The physical conditions are fulfilled for each configuration automatically. This is a consequence of the correct estimates of P_I and u_I given by relations (31), (30).

Shock–bubble interaction

We now consider the test case that is the motivation of this paper, namely the interaction of a shock wave propagating into a heavy fluid and interacting with a bubble of light fluid. The initial situation is represented in figure 1. The results of the two-dimensional direct numerical simulation have already been presented in figures 5, 4 and 6. We now use the one-dimensional model with the same initial conditions and the same mesh (1050 cells). Recall that the two-dimensional computations also used 90 cells in the y-direction. The one-dimensional model being more complicated to solve than the two-dimensional equations, the computational saving with the one-dimensional model is only of a factor 30, instead of the ideal factor of 90. The computational saving would be more spectacular when reducing a three-dimensional problem to a one-dimensional problem.

The one-dimensional model needs no parameters. All terms of discrete equations (24) are now used, including relaxation terms, and rotation entropy creation term. The one-dimensional results are shown in figures 11 and 12 and compared with averaged two-dimensional results. The overall agreement is excellent.

At the first instant, the two volume fraction curves are nearly indistinguishable. More important is the fact that the one-dimensional model is able to predict the peak value which corresponds to an increase compared to the initial value. The local depressurization inside the bubble is correctly predicted by the model. The leading shock wave, as well as the reflected rarefaction wave, are perfectly computed. At the second instant, more discrepancy appears regarding the volume fraction. This is due to the fact that the interface velocity is not single valued in a given section. This is a difficult question not addressed in the present paper. In spite of this difficulty, the average position of the bubble corresponds to the centre of volume predicted by the two-dimensional computations. Also, the area below the volume fraction curve matches the value of the two-dimensional computations. This is also true for the instants 3 and 4 (figure 11c,d). The local depression in the bubble is always

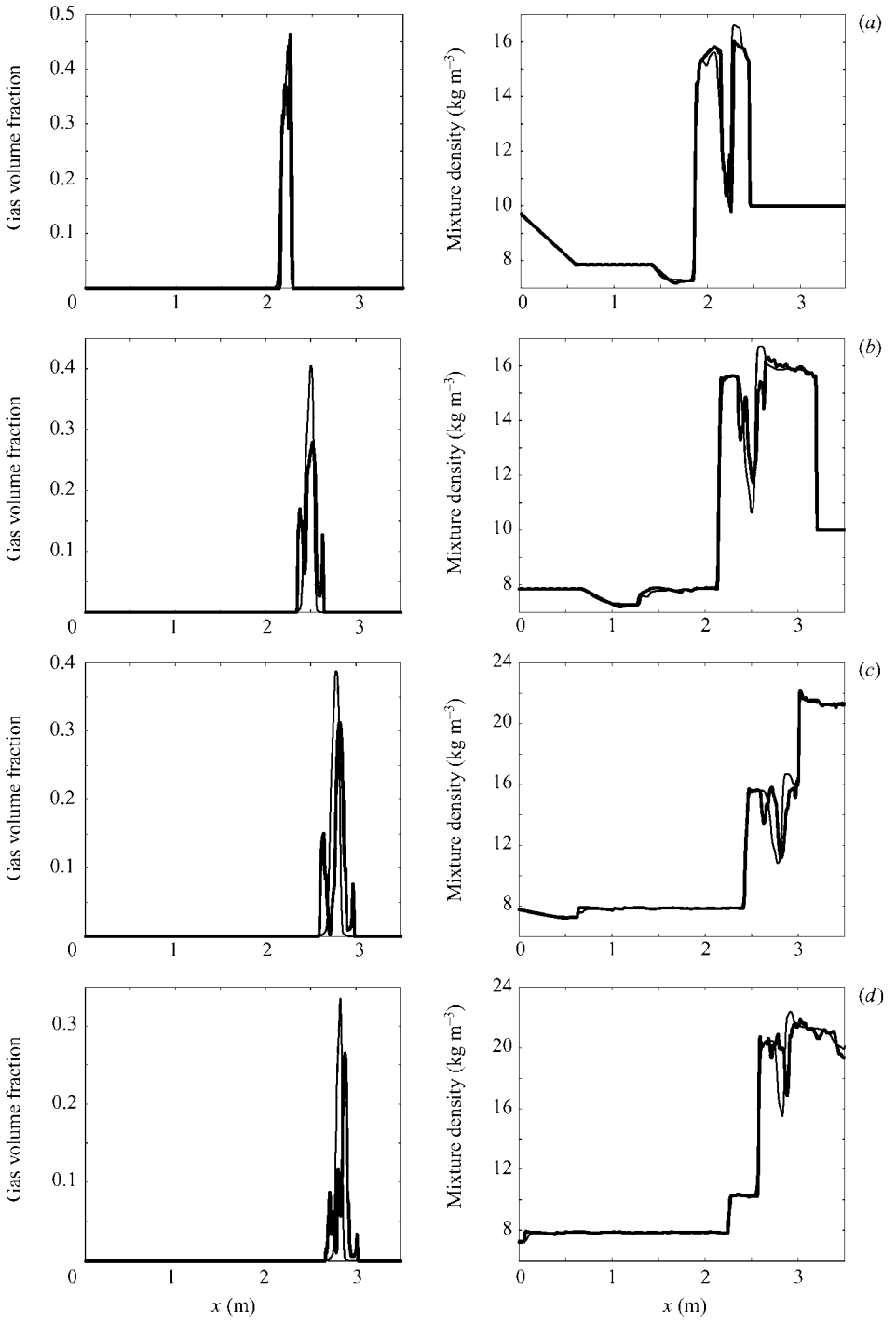

FIGURE 11. Comparison of the one-dimensional model predictions (thin lines) and the two-dimensional averaged results (bold lines) for mixture density and volume fraction at times (*a*) 2.91 ms, (*b*) 5.24 ms, (*c*) 7.66 ms and (*d*) 9.66 ms.

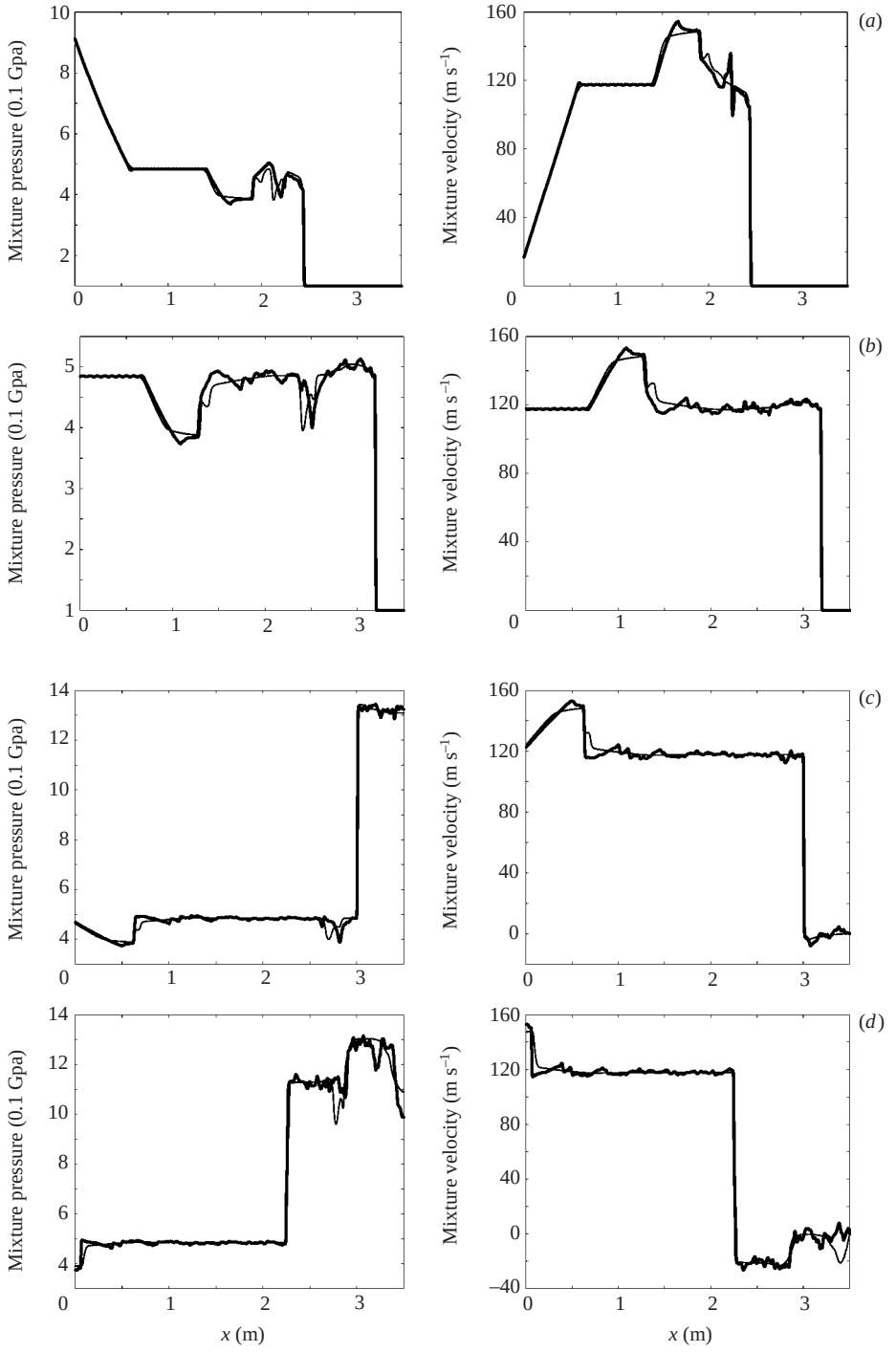

FIGURE 12. Comparison of the one-dimensional model predictions (thin lines) and the two-dimensional averaged results (bold lines) for mixture pressure and velocity at times (*a*) 2.91 ms, (*b*) 5.24 ms, (*c*) 7.66 ms and (*d*) 9.66 ms.

well-predicted, as are the shock and rarefaction wave speeds and magnitudes. This is clear for all variables: velocity, pressures, densities.

The present test corresponds to the incident shock Mach number equal to 1.90. We have made a similar comparison with another shock Mach number 2.50 and the agreement is of the same quality.

9. Conclusions

(i) A hyperbolic model for turbulent multiphase mixtures has been proposed using Hamilton's principle. The model has a clear mathematical structure. The 'interface' pressure and velocity as well as relaxation coefficients should be given *a priori*. In addition to turbulent effects (internal rotation), the inertia effects (bubble pulsations) have been taken into account. By neglecting inertia and turbulence terms we have obtained the Baer–Nunziato model.

(ii) A discrete equation method (DEM) based on averaging of the discrete equations of pure inviscid turbulent fluids has been proposed. It approximates correctly non-conservative terms and involves relaxation parameters intrinsically. For the case of annular flow, a continuous one-dimensional limit of this discrete model has been obtained. The continuous model has the same structure as the system obtained by the variational method, and relaxation coefficients as well as average interface variables (pressure and velocity) have been obtained in explicit form by using this method.

(iii) The model has been validated for a shock–bubble interaction problem where the reference solution is obtained by a direct numerical simulation. The results obtained by the one-dimensional multiphase model are in a very good agreement with the two-dimensional averaged results without using any parameters.

This work has been partially supported by CEA/DIF. The authors are particularly grateful to Serge Gauthier and Denis Souffland. They also address special thanks to Jacques Massoni, Ashwin Chinnayya, Olivier Le Metayer and Eric Daniel of the POLYTECH/INRIA SMASH group for their daily support and help all along this study.

Appendix A. Derivation of Euler–Lagrange equations

To rewrite equations (10) in explicit form, we need to calculate the partial derivatives of Lagrangian (11) with respect to independent variables $\boldsymbol{j}_a$, $\bar{\rho}_a$, etc. We have

$$\frac{\partial L}{\partial \boldsymbol{j}_a} = \boldsymbol{K}_a = \boldsymbol{u}_a + M\frac{\mathrm{d}_1\alpha}{\mathrm{d}t}\frac{\nabla\alpha}{\bar{\rho}_1}\delta_{1a},$$

$$\begin{aligned}\frac{\partial L}{\partial \bar{\rho}_a} &= -\frac{|\boldsymbol{u}_a|^2}{2} + \left(\frac{\partial M}{\partial \bar{\rho}_1}\frac{1}{2}\left(\frac{\mathrm{d}_1\alpha}{\mathrm{d}t}\right)^2 - M\left(\frac{\mathrm{d}_1\alpha}{\mathrm{d}t}\right)\frac{\boldsymbol{j}_1\cdot\nabla\alpha}{\bar{\rho}_1^2}\right)\delta_{1a} \\ &\quad - e_a - \bar{\rho}_a\frac{\partial e_a}{\partial \rho_a}\frac{1}{\alpha_a} - \bar{\rho}_a\frac{\partial e_a}{\partial \eta_a}\left(-\frac{\mathscr{S}_a}{\bar{\rho}_a^2}\right) - \mathscr{T}_a(\Gamma-1)\left(\frac{\bar{\rho}_a}{\alpha_a}\right)^{\Gamma-1}\frac{1}{\bar{\rho}_a} \\ &= -\frac{|\boldsymbol{u}_a|^2}{2} + \left(\frac{\partial M}{\partial \bar{\rho}_1}\frac{1}{2}\left(\frac{\mathrm{d}_1\alpha}{\mathrm{d}t}\right)^2 - M\left(\frac{\mathrm{d}_1\alpha}{\mathrm{d}t}\right)\frac{\boldsymbol{j}_1\cdot\nabla\alpha}{\bar{\rho}_1^2}\right)\delta_{1a} - \mu_a - (\Gamma-1)\frac{k_a}{\rho_a}.\end{aligned}$$

Here $\mu_a = e_a + p_a/\rho_a - \theta_a \eta_a$ is the Gibbs potential. Analogously,

$$\frac{\partial L}{\partial \mathscr{S}_a} = -\bar{\rho}_a \frac{\partial e_a}{\partial \eta_a}\frac{1}{\bar{\rho}_a} = -\frac{\partial e_a}{\partial \eta_a} = -\theta_a,$$

$$\frac{\partial L}{\partial \mathscr{T}_a} = -\left(\frac{\bar{\rho}_a}{\alpha_a}\right)^{\Gamma-1},$$

$$\begin{aligned}\frac{\partial L}{\partial \alpha} &= \frac{1}{2}\frac{\partial M}{\partial \alpha}\left(\frac{\mathrm{d}_1\alpha}{\mathrm{d}t}\right)^2 - \bar{\rho}_1 \frac{\partial e_1}{\partial \rho_1}\frac{\bar{\rho}_1}{\alpha_1^2} + \bar{\rho}_2 \frac{\partial e_2}{\partial \rho_2}\frac{\bar{\rho}_2}{\alpha_2^2} - \mathscr{T}_1\left(\frac{\bar{\rho}_1}{\alpha_1}\right)^{\Gamma-1}(\Gamma-1)\frac{1}{\alpha_1} \\ &\quad + \mathscr{T}_2\left(\frac{\bar{\rho}_2}{\alpha_2}\right)^{\Gamma-1}(\Gamma-1)\frac{1}{\alpha_2} \\ &= p_2 - p_1 + \frac{1}{2}\frac{\partial M}{\partial \alpha}\left(\frac{\mathrm{d}_1\alpha}{\mathrm{d}t}\right)^2 - \mathscr{T}_1\left(\frac{\bar{\rho}_1}{\alpha_1}\right)^{\Gamma-1}(\Gamma-1)\frac{1}{\alpha_1} + \mathscr{T}_2\left(\frac{\bar{\rho}_2}{\alpha_2}\right)^{\Gamma-1}(\Gamma-1)\frac{1}{\alpha_2} \\ &= P_2 - P_1 + \frac{1}{2}\frac{\partial M}{\partial \alpha}\left(\frac{\mathrm{d}_1\alpha}{\mathrm{d}t}\right)^2,\end{aligned}$$

where p_a is the pressures of each component, and we have denoted by P_a the sum of the thermodynamic pressure and the turbulent pressure:

$$P_a = p_a + (\Gamma - 1)\, k_a.$$

Analogously,

$$\frac{\partial L}{\partial \alpha_t} = M\frac{\mathrm{d}_1\alpha}{\mathrm{d}t}, \qquad \frac{\partial L}{\partial \nabla\alpha} = M\frac{\mathrm{d}_1\alpha}{\mathrm{d}t}\boldsymbol{u}_1$$

First, we will transform the equation for the volume concentration:

$$\frac{\partial L}{\partial \alpha} - \frac{\partial}{\partial t}\left(\frac{\partial L}{\partial \alpha_t}\right) - \nabla\cdot\left(\frac{\partial L}{\partial \nabla\alpha}\right) = 0.$$

Taking into account the previous formulae we obtain

$$\frac{\partial}{\partial t}\left(M\frac{\mathrm{d}_1\alpha}{\mathrm{d}t}\right) + \nabla\cdot\left(M\frac{\mathrm{d}_1\alpha}{\mathrm{d}t}\boldsymbol{u}_1\right) = P_2 - P_1 + \frac{1}{2}\frac{\partial M}{\partial \alpha}\left(\frac{\mathrm{d}_1\alpha}{\mathrm{d}t}\right)^2.$$

This equation is the analogue of the Rayleigh–Lamb equation for the case of compressible fluid. It can also be rewritten as

$$\bar{\rho}_1\frac{\mathrm{d}_1}{\mathrm{d}t}\left(\frac{M}{\bar{\rho}_1}\frac{\mathrm{d}_1\alpha}{\mathrm{d}t}\right) = P_2 - P_1 + \frac{1}{2}\frac{\partial M}{\partial \alpha}\left(\frac{\mathrm{d}_1\alpha}{\mathrm{d}t}\right)^2. \tag{A 1}$$

Let us transform the momentum equations:

$$\begin{aligned}&\frac{\partial}{\partial t}(\bar{\rho}_a \boldsymbol{K}_a) + \nabla\cdot(\boldsymbol{j}_a \otimes \boldsymbol{K}_a) - \left(\frac{\partial \boldsymbol{K}_a}{\partial \mathbf{x}}\right)^T \boldsymbol{j}_a - \bar{\rho}_a\, \nabla\left(\frac{\partial L}{\partial\, \bar{\rho}_a}\right) \\ &\quad - \mathscr{S}_a\, \nabla\left(\frac{\partial L}{\partial\, \mathscr{S}_a}\right) - \mathscr{T}_a \nabla\left(\frac{\partial L}{\partial\, \mathscr{T}_a}\right) \\ &= \frac{\partial}{\partial t}(\bar{\rho}_a \boldsymbol{K}_a) + \nabla\cdot(\boldsymbol{j}_a \otimes \boldsymbol{K}_a) - \left(\frac{\partial \boldsymbol{K}_a}{\partial \mathbf{x}}\right)^T \boldsymbol{j}_a\end{aligned}$$

$$+\bar{\rho}_a\,\nabla\left(\frac{|\boldsymbol{u}_a|^2}{2}-\left(\frac{\partial M}{\partial\bar{\rho}_1}\frac{1}{2}\left(\frac{d_1\alpha}{dt}\right)^2-M\left(\frac{d_1\alpha}{dt}\right)\frac{\boldsymbol{j}_1\cdot\nabla\alpha}{\bar{\rho}_1^2}\right)\delta_{1a}\right.$$

$$\left.+\mu_a+(\Gamma-1)\frac{k_a}{\rho_a}\right)+\mathscr{S}_a\nabla\theta_a+\mathscr{T}_a\nabla\left(\left(\frac{\bar{\rho}_a}{\alpha_a}\right)^{\Gamma-1}\right)=0$$

The Gibbs identity (4) implies: $\mathscr{S}_a\nabla\theta_a+\bar{\rho}_a\nabla\mu_a=\alpha_a\nabla p_a$. If we denote the partial turbulent energy $\alpha_a k_a$ by $\overline{k}_a=\mathscr{T}_a(\bar{\rho}_a/\alpha_a)^{\Gamma-1}$, we obtain

$$\bar{\rho}_a\nabla\frac{\partial\overline{k}_a}{\partial\bar{\rho}_a}+\mathscr{T}_a\nabla\frac{\partial\overline{k}_a}{\partial\mathscr{T}_a}=\nabla\left(\bar{\rho}_a\frac{\partial\overline{k}_a}{\partial\bar{\rho}_a}+\mathscr{T}_a\frac{\partial\overline{k}_a}{\partial\mathscr{T}_a}-\overline{k}_a\right)+\frac{\partial\overline{k}_a}{\partial\alpha_a}\nabla\alpha_a$$

$$=\nabla\left(\bar{\rho}_a\frac{\partial\overline{k}_a}{\partial\bar{\rho}_a}\right)+\frac{\partial\overline{k}_a}{\partial\alpha_a}\nabla\alpha_a=\nabla\left((\Gamma-1)\alpha_a k_a\right)-(\Gamma-1)k_a\nabla\alpha_a.$$

These expressions permit us to simplify the momentum equations:

$$\frac{\partial}{\partial t}(\bar{\rho}_a\boldsymbol{K}_a)+\nabla\cdot(\boldsymbol{j}_a\otimes\boldsymbol{K}_a+\alpha_a P_a)-P_a\nabla\alpha_a-\left(\frac{\partial\boldsymbol{K}_a}{\partial\mathbf{x}}\right)^T\boldsymbol{j}_a$$

$$+\bar{\rho}_a\,\nabla\left(\frac{|\boldsymbol{u}_a|^2}{2}-\left(\frac{\partial M}{\partial\bar{\rho}_1}\frac{1}{2}\left(\frac{d_1\alpha}{dt}\right)^2-\frac{M}{\bar{\rho}_1}\left(\frac{d_1\alpha}{dt}\right)\boldsymbol{u}_1\cdot\nabla\alpha\right)\delta_{1a}\right)=0.$$

By using the definition of $\boldsymbol{K}_a$:

$$\boldsymbol{K}_a=\boldsymbol{u}_a+\frac{M}{\bar{\rho}_1}\frac{\mathrm{d}_1\alpha}{\mathrm{d}t}\nabla\alpha\;\delta_{1a},$$

and the Rayleigh–Lamb equation (A 1), the equation of balance for momentum becomes

$$\bar{\rho}_a\frac{\mathrm{d}_a\boldsymbol{u}_a}{\mathrm{d}t}+\alpha_a\nabla P_a+\delta_{1a}(P_2-P_1)\nabla\alpha+\delta_{1a}\nabla\left(\left(M-\bar{\rho}_1\frac{\partial M}{\partial\bar{\rho}_1}\right)\frac{1}{2}\left(\frac{\mathrm{d}_1\alpha}{\mathrm{d}t}\right)^2\right)=0.\quad\text{(A 2)}$$

The energy equations for each component $a=1,2$, which are consequences of the entropy equations

$$\frac{\mathrm{d}_a\eta_a}{\mathrm{d}t}=0,\quad\frac{\mathrm{d}_a\varkappa_a}{\mathrm{d}t}=0$$

can be rewritten as

$$\frac{\partial}{\partial t}\left(\frac{|\boldsymbol{j}_a|^2}{2\bar{\rho}_a}+\bar{\rho}_a e_a+\alpha_a k_a+\frac{M}{2}\left(\frac{\mathrm{d}_1\alpha}{\mathrm{d}t}\right)^2\delta_{1a}\right)+\nabla\cdot\left(\boldsymbol{u}_a\left(\frac{\bar{\rho}_a|\boldsymbol{u}_a|^2}{2}+\bar{\rho}_a e_a\right.\right.$$

$$\left.\left.+\left(2M-\bar{\rho}_1\frac{\partial M}{\partial\bar{\rho}_1}\right)\frac{1}{2}\left(\frac{\mathrm{d}_1\alpha}{\mathrm{d}t}\right)^2\delta_{1a}+\alpha_a(k_a+P_a)\right)\right)=-P_2\frac{\partial\alpha_a}{\partial t}.\quad\text{(A 3)}$$

Here δ_{1a} is the Kronecker symbol. The energy due to the pulsations of the dispersed phase is only in the equation of the energy of the continuous phase. Rewriting momentum equations (A 2) and (A 3) in 'conservative' form, we obtain system (13).

Flow pattern	Length of contact	Indicator function X_1^*	Riemann problem flux
1 - 2	$H\mathrm{Max}(0;\alpha_{1,i-1}-\alpha_{1,i})$	$X_1^*(1,2)=\begin{cases}1 & \text{if } u^*(1,2)>0\\ 0 & \text{otherwise}\end{cases}$	$\boldsymbol{F}^*(1,2)$
1 - 1	$H\mathrm{Min}(\alpha_{1,i-1};\alpha_{1,i})$	$X_1^*(1,1)=1$	$\boldsymbol{F}^*(1,1)$
2 - 1	$H\mathrm{Max}(0;\alpha_{1,i}-\alpha_{1,i-1})$	$X_1^*(2,1)=\begin{cases}1 & \text{if } u^*(2,1)<0\\ 0 & \text{otherwise}\end{cases}$	$\boldsymbol{F}^*(2,1)$
2 - 2	$H\mathrm{Min}(\alpha_{2,i-1};\alpha_{2,i})$	$X_1^*(2,2)=0$	$\boldsymbol{F}^*(2,2)$

TABLE 1. The various flow situations on the left-hand cell boundary and the ingredients for the flux computation of fluid 1. The asterisk denotes the solution of the Riemann problem.

Appendix B. Calculation of the five integrals of the discrete equations method

Numerical approximation of the temporal term

For clarity, we consider fluid 1. We begin with the first integral:

$$\boldsymbol{I}_1=\int_0^{\Delta t}\int_{C_i}\left(\frac{\partial X_1\boldsymbol{W}_1}{\partial t}\right)\mathrm{d}x\,\mathrm{d}y\,\mathrm{d}s=\int_{C_i}\int_0^{\Delta t}\left(\frac{\partial X_1\boldsymbol{W}_1}{\partial t}\right)\mathrm{d}x\,\mathrm{d}y\,\mathrm{d}s$$
$$=\int_0^{H}\int_{-\Delta x/2}^{+\Delta x/2}\left((X\boldsymbol{W})_{1,i}^{n+1}-(X\boldsymbol{W})_{1,i}^{n}\right)\mathrm{d}x\,\mathrm{d}y$$

which can be written in the form

$$\boldsymbol{I}_1=H\Delta x\left((\alpha\overline{\overline{\boldsymbol{W}}})_{1,i}^{n+1}-(\alpha\overline{\overline{\boldsymbol{W}}})_{1,i}^{n}\right).$$

Numerical approximation of the convective fluxes

We now consider the second integral:

$$\boldsymbol{I}_2=\int_0^{\Delta t}\int_0^{H}\left((X\boldsymbol{F})_{1,i+1/2}-(X\boldsymbol{F})_{1,i-1/2}\right)\mathrm{d}y\,\mathrm{d}t=\Delta t\,H\left(\widetilde{\langle X\boldsymbol{F}\rangle}_{1,i+1/2}-\widetilde{\langle X\boldsymbol{F}\rangle}_{1,i-1/2}\right).$$

We focus on the flux $\int_0^H(X\boldsymbol{F})_{1,i-1/2}\,\mathrm{d}y$. In order to compute this integral, four cases have to be considered, according to the location of the fluid in contact at the cell boundary (see figure 7). These four cases are summarized in table 1.

The function $X_1^*(p,q)$ represents the fluid indicator function at the cell boundary, where fluid p is initially on the left of the cell boundary and fluid q on the right. When fluid 1 is in contact with itself, this function is always equal to 1. Inside fluid 2, the indicator function of fluid 1 is always 0. When fluid 2 is in contact with itself, the indicator function of fluid 1 is always 0: $X_1^*(2,2)=0$. When fluid 1 is in contact with fluid 2, or inversely, the indicator function at the cell boundary depends on the sign of the interface velocity. The interface velocity $u^*(p,q)$ is determined by solving the Riemann problem between the two fluids in contact. This velocity is determined from an appropriate Riemann solver for the k-model. Such a solver is derived in § 5. We define flux $\boldsymbol{F}_{i-1/2}^*(p,q)$ at the interface $i-1/2$ when the left-hand state is made of fluid p and the right-hand state of fluid q. The flux is also determined by the Riemann solver. The length of contact corresponds to the height of contact between fluids at the cell boundary for the flow pattern (p,q). By summing the four fluxes weighted by the corresponding length and indicator, we find the total flux for fluid 1

at the cell boundary $i-1/2$:

$$\int_0^H (X\boldsymbol{F})_{1,i-1/2}\,\mathrm{d}y = X^*_{1,i-1/2}(1,2)H\mathrm{Max}(0;\alpha_{1,i-1}-\alpha_{1,i})\boldsymbol{F}^*_{i-1/2}(1,2) + X^*_{1,i-1/2}(1,1)H\mathrm{Min}(\alpha_{1,i-1};\alpha_{1,i})\boldsymbol{F}^*_{i-1/2}(1,1) + X^*_{1,i-1/2}(2,1)H\mathrm{Max}(0;\alpha_{1,i}-\alpha_{1,i-1})\boldsymbol{F}^*_{i-1/2}(2,1).$$

Similarly at cell boundary $(i+1/2)$ the total flux for fluid 1 is

$$\int_0^H (X\boldsymbol{F})_{1,i+1/2}\,\mathrm{d}y = X^*_{1,i+1/2}(1,2)H\mathrm{Max}(0;\alpha_{1,i}-\alpha_{1,i+1})\boldsymbol{F}^*_{i+1/2}(1,2) + X^*_{1,i+1/2}(1,1)H\mathrm{Min}(\alpha_{1,i+1};\alpha_{1,i})\boldsymbol{F}^*_{i+1/2}(1,1) + X^*_{1,i+1/2}(2,1)H\mathrm{Max}(0;\alpha_{1,i+1}-\alpha_{1,i})\boldsymbol{F}^*_{i+1/2}(2,1).$$

It remains to determine the numerical approximation of integral $\boldsymbol{I}_3$. For the sake of clarity we again use the index a for the characteristic function X_a. We have

$$\boldsymbol{I}_3 = \int_0^{\Delta t}\int_{C_i} \frac{\partial X_a \boldsymbol{G}}{\partial y}\,\mathrm{d}x\,\mathrm{d}y\,\mathrm{d}s.$$

This yields for fluid 1

$$\boldsymbol{I}_3 = \int_0^{\Delta t}\int_{-\Delta x/2}^{+\Delta x/2} (X_1|_{y=H}\boldsymbol{G}^*_i - X_1|_{y=0}\boldsymbol{G}^*_i)\,\mathrm{d}x\,\mathrm{d}t.$$

As shown in figure 7, $X_1|_{y=H}=1$ and $X_1|_{y=0}=1$. At the top and bottom boundaries, corresponding to walls, the flux reduces to $\boldsymbol{G}=(0,0,0,P,0,0)^T$ and the difference $\boldsymbol{I}_3$ cancels. This is because the initial y-velocity component is zero. When the flow is initially one-dimensional (zero vertical velocity), it remains one-dimensional during the time evolution because the flux difference $\boldsymbol{I}_3$ vanishes. For fluid 2, $X_2|_{y=H}=0$ and $X_2|_{y=0}=0$ so that $\boldsymbol{I}_3$ vanishes again. Thus, for both fluids:

$$\boldsymbol{I}_3 = \boldsymbol{0}$$

Numerical approximation of the non-conservative terms

Following the same guidelines as previously, we first consider the integral $\boldsymbol{I}_4$.

$$\boldsymbol{I}_4 = \int_0^{\Delta t}\int_{C_i} \boldsymbol{F}^{lag}\frac{\partial X_1}{\partial x}\,\mathrm{d}x\,\mathrm{d}y\,\mathrm{d}s.$$

As shown in figure 7 there are at the most six internal interfaces inside the two-phase control volume C_i. The first four interfaces are the right- and left-hand cell boundaries, while the last two interfaces correspond to the horizontal fluid layer inside the cell. When considering the integral $\boldsymbol{I}_4$ the term associated with the horizontal interface cancels because $[X_1]=0$. Only the four vertical interfaces must be considered. Thus we need to compute

$$\boldsymbol{I}_4 = \int_0^{\Delta t}\left(\int_0^H \boldsymbol{F}^{lag}_{i-1/2}[X_1]_{i-1/2}\,\mathrm{d}y + \int_0^H \boldsymbol{F}^{lag}_{i+1/2}[X_1]_{i+1/2}\,\mathrm{d}y\right)\mathrm{d}t.$$

By using the definition of the averages (26), this relation can be rewritten as

$$\boldsymbol{I}_4 = H\,\Delta t\left(\langle\widetilde{\boldsymbol{F}^{lag}}[X_1]\rangle_{i-1/2} + \langle\widetilde{\boldsymbol{F}^{lag}}[X_1]\rangle_{i+1/2}\right).$$

Flow pattern	Length of contact	$[X_1^*]$	$\boldsymbol{F}^{lag,*}$
1 - 2	$H\mathrm{Max}(0;\alpha_{1,i-1}-\alpha_{1,i})$	$-\dfrac{u^{*,+}(1,2)}{\lvert u^*(1,2)\rvert}$	$\boldsymbol{F}^{lag,*}(1,2)$
1 - 1	$H\mathrm{Min}(\alpha_{1,i-1};\alpha_{1,i})$	0	$\boldsymbol{F}^{lag,*}(1,1)$
2 - 1	$H\mathrm{Max}(0;\alpha_{1,i}-\alpha_{1,i-1})$	$\dfrac{u^{*,+}(2,1)}{\lvert u^*(2,1)\rvert}$	$\boldsymbol{F}^{lag,*}(2,1)$
2 - 2	$H\mathrm{Min}(\alpha_{2,i-1},\alpha_{2,i})$	0	$\boldsymbol{F}^{lag,*}(2,2)$

TABLE 2. The various 'non-conservative products' for the inner interface from the left cell boundary.

We detail the integral calculation for the interfaces from the left-hand cell boundary. The same four possible cases that have been considered for the flux computation are summarized in table 2. For each interface (contact) from the left-hand cell boundary, the jump of the phase function $[X_1^*]$ is computed according to the sign of the interface velocity, the solution of the Riemann problem. For instance, for the flow pattern (1—2), the jump $[X_1^*]$ is equal to -1 when the interface velocity between fluids 1 on the left and 2 on the right is positive. Indeed, $X_1=0$ in fluid 2, and $X_1=1$ in fluid 1. Thus, the jump is -1 when fluid 1 is entering the cell. When it exits the cell the jump is zero. This is summarized by the interface velocity $u^*(1,2)$, where the asterisk represents the Riemann problem solution. The positive part of this velocity is denoted $u^{*,+}(1,2)$. Regarding the flow pattern 1-1, the jump $[X_1^*]$ is always zero, since there is no interface for this configuration. Consequently,

$$\int_0^H \boldsymbol{F}^{lag}_{i-1/2}[X_1]_{i-1/2}\,\mathrm{d}y = H\begin{pmatrix}[X_1^*]_{i-1/2}(1,2)\,\mathrm{Max}(0;\alpha_{1,i-1}-\alpha_{1,i})\boldsymbol{F}^{lag,*}_{i-1/2}(1,2)\\ +[X_1^*]_{i-1/2}(2,1)\,\mathrm{Max}(0;\alpha_{1,i}-\alpha_{1,i-1})\boldsymbol{F}^{lag,*}_{i-1/2}(2,1)\end{pmatrix}.$$

By using the definition of the surface and time averages respectively we obtain under the CFL restriction:

$$\begin{aligned}\langle\widetilde{\boldsymbol{F}^{lag}[X_1]}\rangle_{i-1/2} &= [X_1^*]_{i-1/2}(1,2)\,\mathrm{Max}(0;\alpha_{1,i-1}-\alpha_{1,i})\boldsymbol{F}^{lag,*}_{i-1/2}(1,2)\\ &\quad+[X_1^*]_{i-1/2}(2,1)\,\mathrm{Max}(0;\alpha_{1,i}-\alpha_{1,i-1})\boldsymbol{F}^{lag,*}_{i-1/2}(2,1).\end{aligned}$$

Regarding the interface coming from the right-hand boundary, a similar calculation is made:

$$\begin{aligned}\langle\widetilde{\boldsymbol{F}^{lag}[X_1]}\rangle_{i+1/2} &= [X_1^*]_{i+1/2}(1,2)\,\mathrm{Max}(0;\alpha_{1,i}-\alpha_{1,i+1})\boldsymbol{F}^{lag,*}_{i+1/2}(1,2)\\ &\quad+[X_1^*]_{i+1/2}(2,1)\,\mathrm{Max}(0;\alpha_{1,i+1}-\alpha_{1,i})\boldsymbol{F}^{lag,*}_{i+1/2}(2,1).\end{aligned}$$

It remains to determine the numerical approximation of the last integral $\boldsymbol{I}_5$:

$$\boldsymbol{I}_5=\int_0^{\Delta t}\int_{C_i}\boldsymbol{G}^{lag}\frac{\partial X}{\partial y}\,\mathrm{d}x\,\mathrm{d}y\,\mathrm{d}t=\int_0^{\Delta t}\int_0^{\Delta x}\sum\boldsymbol{G}^{lag}[X_1]\,\mathrm{d}x\,\mathrm{d}t.$$

The jump $[X_1]$ is non-zero only for the horizontal interfaces (see figure 7). Thus the approximation of $\boldsymbol{I}_5$ is

$$\boldsymbol{I}_5=\Delta t\Delta x(\langle\widetilde{\boldsymbol{G}^{lag,*}}\rangle_i(2,1)-\langle\widetilde{\boldsymbol{G}^{lag,*}}\rangle_i(1,2)).$$

The fourth component of $\boldsymbol{I}_5$ is the pressure difference. It cancels when the initial vertical velocity is zero.

REFERENCES

Abgrall, R. 1996 How to prevent pressure oscillations in multicomponent flow calculations: A quasi conservative approach. *J. Comput. Phys.* **125**, 150–160.

Abgrall, R. & Saurel, R. 2003 Discrete equations for physical and numerical compressible multiphase mixtures. *J. Comput. Phys.* **186**, 361–396.

Baer, M. & Nunziato, J. 1986 A two-phase mixture theory for the deflagration-to-detonation transition (DDT) in reactive granular materials. *Intl J. Multiphase Flows* **12**, 861–889.

Bdzil, J., Menikoff, R., Son, S., Kapila, A. & Steward, D. 1999 Two-phase modeling of a deflagration-to-detonation transition in granular materials: A critical exmination of modeling issues. *Phys. Fluids* **11**, 378–402.

Chen, Y., Glimm, J., Sharp, D. & Zhang, Q. 1996 A two-phase flow model of the Rayleigh-Taylor mixing zone. *Phys. Fluids* **8**, 816–825.

Dalmaso, G., LeFloch, P. & Murat, F. 1995 Definition and weak stability of non-conservative products. *J. Math. Pures Appl.* **74**, 483–548.

Declerc, E., Forestier, A., Herard, J., Louis, X. & Poissant, G. 2001 An exact Riemann solver for a multicomponent turbulent flow. *Intl J. Comput. Fluid Dyn.* **14**, 117–131.

Drew, D. & Passman, S. 1998 *Theory of Multicomponent Fluids.* Springer.

Fedkiw, R., Aslam, T., Merriman, B. & Osher, S. 1999 A non oscillatory eulerian approach to interfaces in multimaterial flows (The Ghost-Fluid Method). *J. Computat. Phys.* **152**, 457–492.

Gardner, C., Glimm, J., McBryan, O., Menikoff, R., Sharp, D. & Zhang, Q. 1988 The dynamics of bubble growth for the Rayleigh-Taylor unstable interfaces. *Phys. Fluids* **31**, 447–465.

Gavrilyuk, S. & Gouin, H. 1999 A new form of governing equations of fluids arising from Hamilton's principle. *Intl J. Engng Sci.* **37**, 1495–1520.

Gavrilyuk, S. & Saurel, R. 2002 Mathematical and numerical modeling of two-phase compressible flows with micro-inertia. *J. Computat. Phys.* **175**, 326–360.

Glimm, J., Li, X., Menikoff, R., Sharp, D. & Zhang, Q. 1990 A numerical study of bubble interactions in Rayleigh-Taylor instability for compressible fluids. *Phys. Fluids* A **2**, 2046–2054.

Glimm, J., Saltz, D. & Sharp, D. 1999 Two-phase modelling of a fluid mixing layer. *J. Fluid Mech.* **378**, 119–143.

Godunov, S., Zabrodin, A., Ivanov, M., Kraiko, A. & Prokopov, G. 1979 *Resolution Numerique des Problemes Multidimensionnels de la Dynamique des Gaz*. Moscow: Editions Mir.

Hou, T. & LeFloch, P. 1994 Why non-conservative schemes converge to the wrong solution: Error analysis. *Math. Comput.* **62**, 497–530.

Kapila, A., Menikoff, R., Bdzil, J., Son, S. & Stewart, D. 2001 Two-phase modeling of DDT in granular materials: reduced equations. *Phys. Fluids* **13**, 3002–3024.

Kapila, A., Son, S., Bdzil, J., Menikoff, R. & Stewart, D. 1997 Two-phase modeling of DDT: structure of the velocity-relaxation zone. *Phys. Fluids* **9**, 3885–3897.

Karni, S. 1994 Multicomponent flow calculations by a consistent primitive algorithm. *J. Comput. Phys.* **112**, 31–43.

Karni, S. 1996 Hybrid multifluid algorithms. *SIAM J. Sci. Comput.* **17**, 1019–1039.

Lamb, H. 1932 *Hydrodynamics.* Cambridge University Press.

Massoni, J., Saurel, R., Nkonga, B. & Abgrall, R. 2002 Proposition de methodes et modeles euleriens pour les problemes a interfaces entre fluides compressibles en presence de transfert de chaleur. *Intl J. Heat Mass Transfer* **45**, 1287–1307.

Nguyen, D., Gibou, F. & Fedkiw, R. 2002 A fully conservative ghost fluid method and stiff detonation waves. *Proc. Twelfth Detonation Symp. (Intl), San Diego* (to appear).

Saurel, R. & Abgrall, R. 1999*a* A multiphase Godunov method for compressible multifluid and multiphase flows. *J. Comput. Phys.* **150**, 425–467.

Saurel, R. & Abgrall, R. 1999*b* A simple method for compressible multifluid flows. *SIAM J. Sci. Comput.* **21**, 1115–1145.

Saurel, R. & LeMetayer, O. 2001 A multiphase model for compressible flows with interfaces, shocks, detonation waves and cavitation. *J. Fluid Mech.* **431**, 239–271.

Serrin, J. 1959 Mathematical principles of classical fluid mechanics. In *Enyclopedia of Physics* VIII/1 S. Flugge (ed.). Springer.

Shyue, K. 1998 An efficient shock-capturing algorithm for compressible multicomponent problems. *J. Comput. Phys.* **142**, 208–242.

Stewart, H. & Wendroff, B. 1984 Two-phase flow: Models and methods. *J. Comput. Phys.* **56**, 363–409.

Toro, E. 1997 *Riemann Solvers and Numerical Methods for Fluid Dynamics.* Springer.

Wilcox, D. 1998 *Turbulence Modeling for* CFD. DCW Industries.

Youngs, D. 1984 Numerical simulation of turbulent mixing by Rayleigh-Taylor instability. *Physica* D **12**, 32–44.

Youngs, D. 1989*a* Modeling turbulent mixing by Rayleigh-Taylor instability. *Physica* D **37**, 270–287.

Youngs, D. 1989*b* Three-dimensional numerical simulation of turbulent mixing by Rayleigh–Taylor instability. *Phys. Fluids* A **3**, 1312–1319.